© 2014. Published by The Company of Biologists Ltd | Journal of Cell Science (2014) 127, 3720–3734 doi:10.1242/jcs.148619

RESEARCH ARTICLE

Probing the biomechanical contribution of the endothelium to lymphocyte migration: diapedesis by the path of least resistance

Roberta Martinelli[1,2], Adam S. Zeiger[3], Matthew Whitfield[3], Tracey E. Sciuto[4], Ann Dvorak[4], Krystyn J. Van Vliet[3,5], John Greenwood[2,*] and Christopher V. Carman[1,*]

ABSTRACT

Immune cell trafficking requires the frequent breaching of the endothelial barrier either directly through individual cells ('transcellular' route) or through the inter-endothelial junctions ('paracellular' route). What determines the loci or route of breaching events is an open question with important implications for overall barrier regulation. We hypothesized that basic biomechanical properties of the endothelium might serve as crucial determinants of this process. By altering junctional integrity, cytoskeletal morphology and, consequently, local endothelial cell stiffness of different vascular beds, we could modify the preferred route of diapedesis. In particular, high barrier function was associated with predominantly transcellular migration, whereas negative modulation of junctional integrity resulted in a switch to paracellular diapedesis. Furthermore, we showed that lymphocytes dynamically probe the underlying endothelium by extending invadosome-like protrusions (ILPs) into its surface that deform the nuclear lamina, distort actin filaments and ultimately breach the barrier. Fluorescence imaging and pharmacologic depletion of F-actin demonstrated that lymphocyte barrier breaching efficiency was inversely correlated with local endothelial F-actin density and stiffness. Taken together, these data support the hypothesis that lymphocytes are guided by the mechanical 'path of least resistance' as they transverse the endothelium, a process we term 'tenertaxis'.

KEY WORDS: Actin, Barrier, Endothelium, Leukocyte, Migration, Stiffness

INTRODUCTION

The vascular endothelium represents one of the crucial barriers of the body, providing the partition between two of its key compartments – the blood circulation and the underlying tissue. The primary function of the endothelium is to restrict the movement of fluid, solutes and cells into and out of the tissues (Dudek and Garcia, 2001; Mehta and Malik, 2006). Immune cells (i.e. blood leukocytes) could be regarded as 'professional invasive cells', with the need to efficiently and repeatedly cross this barrier. Lymphocytes are particularly adept at trafficking in and out of diverse tissues during hematopoiesis, immunosurveillance and inflammatory responses (von Andrian and Mackay, 2000). Through the expression of appropriate adhesion molecules and chemoattractants, the endothelium actively establishes zones within the vasculature that support leukocyte adhesion (Ley et al., 2007; von Andrian and Mackay, 2000). However, the mechanisms that control the crucial step of formally breaching the endothelial barrier (i.e. 'transmigration' or 'diapedesis') are still incompletely understood. In particular, it is unclear how the specific site for a barrier-breaching event is determined.

It was once held that sites for diapedesis were limited to segments of inter-endothelial junctions. Thus, 'paracellular' diapedesis gaps were formed as a result of leukocyte-driven protrusive forces, aided by endothelial-mediated remodeling of actin and adherens and tight junction complexes (Muller, 2003; Turowski et al., 2008). Recently, it has become clear that a quantitatively important alternative, junction-independent, 'transcellular' mode of diapedesis exists. Here, individual leukocytes pass directly through the body of individual endothelial cells (Bamforth et al., 1997; Carman, 2009; Carman and Springer, 2004; Cinamon et al., 2004; Feng et al., 1998; Wolburg et al., 2005; Yang et al., 2005). This raises important new questions, such as what determines the precise subcellular locus in an endothelial breaching event, why two routes exist and what governs the usage of one mode over the other.

An interesting, but largely unexplored, hypothesis is that basic biomechanical features, such as the local intercellular junction tightness and endothelial cell stiffness, play a role in determining the route and location of diapedesis. Several investigators have suggested that leukocyte transmigration sites might simply represent the path of least resistance, implying that spatiotemporal differences in the physical or biomechanical strength of the endothelial barrier crucially influence where leukocytes ultimately undergo diapedesis (Kvietys and Sandig, 2001; Lossinsky and Shivers, 2004). Although this idea is elegantly simple and intuitive, it remains to be directly tested.

In the current study we demonstrate, by using endothelial cell models of differing junctional integrity, along with a range of junctional-integrity- and cytoskeleton-modulating stimuli, that lymphocyte migration-route preference can be switched. Furthermore, through combined fluorescence, electron and atomic force microscopy, we define a dynamic 'invadosome-like protrusion' (ILP)-mediated process of actively seeking out 'soft' (Latin, *tener*) spots for diapedesis; a process that we term 'tenertaxis'. Our findings in support of a path-of-least-resistance hypothesis have important implications for understanding the

[1]Center for Vascular Biology Research, Department of Medicine, Beth Israel Deaconess Medical Center and Harvard Medical School, Boston, MA 02215, USA. [2]Department of Cell Biology, Institute of Ophthalmology, UCL, 11-43 Bath Street, London EC1V 9EL, UK. [3]Department of Materials Science & Engineering, Massachusetts Institute of Technology, Cambridge, MA 02139, USA. [4]Center for Vascular Biology Research, Department of Medicine, Beth Israel Deaconess Medical Center and Harvard Medical School, Boston, MA 02215, USA. [5]Department of Biological Engineering, Massachusetts Institute of Technology, Cambridge, MA 02139, USA.

*Authors for correspondence (j.greenwood@ucl.ac.uk; ccarman@bidmc.harvard.edu)

Received 6 January 2014; Accepted 19 June 2014

Journal of Cell Science

Journal of Cell Science (2014) 127, 3720–3734 doi:10.1242/jcs.148619

relationship between leukocyte trafficking and the regulation of fluid and solute permeability by endothelia.

RESULTS

Correlation between junctional integrity and the route of diapedesis in different vascular endothelia

The overall integrity of the vascular endothelium depends largely on its intercellular adherens and tight junctions and associated cortical actin filaments (Bazzoni and Dejana, 2004; Spindler et al., 2010; Wojciak-Stothard and Ridley, 2002). The relative strength of these junctional complexes determines the barrier properties with respect to fluid and solutes, and can be measured by trans-endothelial electrical resistance (TEER) (Mehta and Malik, 2006). As a starting point for assessing the relationship between junctional integrity and the route of diapedesis, we examined TEER in endothelia from different vascular beds (that were activated for 24 h with TNF-α to model settings of inflammatory lymphocyte recruitment). TEER of primary rat brain microvascular endothelial cells (MVECs) was predictably high (~77 Ωcm^2), whereas that of primary rat heart MVECs was significantly lower (~25 Ωcm^2; Fig. 1A). Human heart and lung MVECs also showed significantly lower TEER compared with that of brain endothelial cells (Fig. 1A).

Next, we determined the route of primary effector lymphocyte diapedesis on these differing endothelia through fixed end-point high-resolution fluorescence image analysis (Fig. 1B). Consistent with previous *in vivo* studies (Wolburg et al., 2005), we found that migration across brain MVECs proceeded more slowly than across peripheral endothelia. On peripheral MVECs, by 10 min, ~40–50% of T cells had breached the endothelium and were actively transmigrating (Fig. 1C; as defined in Materials and Methods; supplementary material Fig. S1A), and the level of total diapedesis (the combined fraction of T cells that were transmigrating or had already completed transmigration) was ~70–80% (supplementary material Fig. S1A,B). On brain MVECs, the fractions of transmigrating T cells and total diapedesis were only ~20% (Fig. 1C) and 25% (supplementary material Fig. S1B), respectively, after 10 min, and a total duration of 30 min was required to achieve levels that were comparable to those seen on peripheral MVECs (Fig. 1C; supplementary material Fig. S1B). Detailed examination of the transmigrating population of T cells demonstrated that the majority of diapedesis events on rat heart, human heart and human lung MVECs were paracellular, whereas, on rat brain MVECs (whether examined at 10 or 30 min), it was mostly transcellular (Fig. 1Di–ii). Comparative analysis showed that the average cell area and junctional perimeter length were

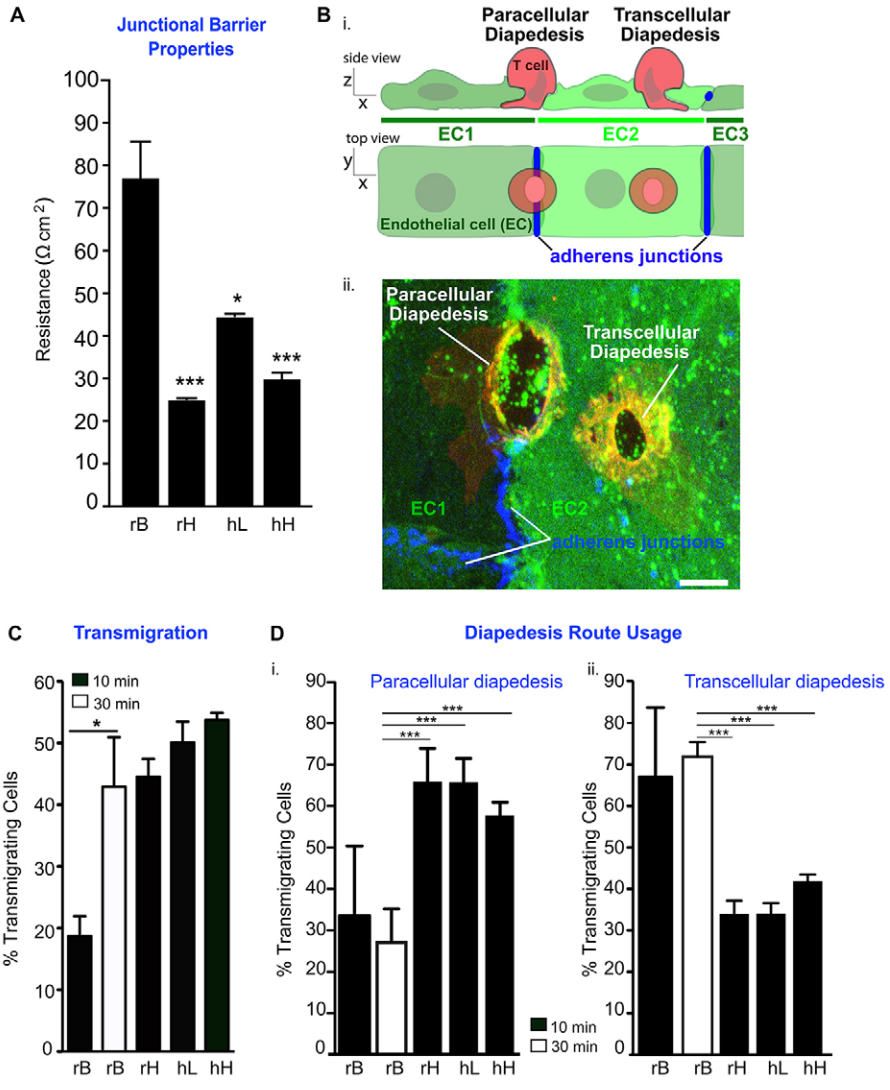

Fig. 1. Assessment of junctional integrity and diapedesis route preference in different vascular endothelial monolayers. Primary rat brain (rB), rat heart (rH), human lung (hL) and human heart (hH) MVECs were grown to confluence and stimulated with TNF-α (24 h) before (A) measuring basal TEER or (B–D) addition of rat or human T cells for 10 min (black bars; all endothelial cells) or 30 min (white bars; rat brain MVECs only), prior to fixation and staining with antibodies against VEC (blue), ICAM-1 (green) and LFA-1 (red). (B) Schematic (i) and representative confocal imaging (ii) of paracellular and transcellular diapedesis events. Scale bar: 5 μm. (C) Quantification of 'transmigrating' cells (see scheme in supplementary material Fig. S1A). (D) Quantification of relative paracellular (i) and transcellular (ii) diapedesis. Data show the mean±s.e.m. (at least four separate experiments); *$P<0.05$, ***$P<0.001$.

Journal of Cell Science (2014) 127, 3720–3734 doi:10.1242/jcs.148619

essentially identical for rat brain and heart MVECs (supplementary material Fig. S1C), indicating that differences in route usage in the endothelia cannot be ascribed to geometrical parameters. These results support the idea that tighter junctions favor transcellular migration by lymphocytes.

The effect of junctional modifying agents on the route of migration

To test this idea further, we investigated the effects of junctional enhancing or disrupting agents on the route of migration. To increase junctional integrity, we used adrenomedullin and the cAMP analog 8-pCPT-2′-O-Me-cAMP (O-Me). Whereas adrenomedullin is a crucial autocrine and paracrine hormone mediator of blood–brain-barrier junctional tightness (Kis et al., 2003), O-Me acts downstream of adrenomedullin by directly stimulating the guanine nucleotide exchange factor EPAC-1 (also known as RAPGEF3), which, in turn, activates the small GTPase Rap-1 and, ultimately, Rac-1 (Bos, 2003; Spindler et al., 2010). Addition of adrenomedullin or O-Me to rat brain endothelium led to a ∼15% enhancement in the already high (∼77 Ωcm^2) resistance (Fig. 2A) and a detectable increase in the amount of cortical F-actin (Fig. 2B, white arrowheads). The adherens junction protein VE-cadherin (VEC, also known as cadherin-5) showed similarly strong and continuous or linear staining under control, adrenomedullin-treated and O-Me-treated conditions (Fig. 2B). By contrast, to decrease barrier function we used histamine, which stimulates RhoA, stress fibers and contractility (Wojciak-Stothard and Ridley, 2002). On rat brain endothelium, histamine only induced a minimal change in barrier function (Fig. 2A) and a modest loss of cortical actin and increase in stress fibers, with no obvious change in VEC distribution (Fig. 2B). Thus, we turned to a pharmacological approach, using the src inhibitor PP2 to block the requisite phosphorylation of the Rac-1 effector cortactin, which is crucial for cortical actin assembly (Pendyala et al., 2008). Addition of PP2 (10 μM) induced a substantial decrease in barrier function (Fig. 2A), along with decreased levels of cortical actin, increased stress fibers, discontinuous VEC and the formation of gaps (Fig. 2B, yellow arrowheads; quantification in Fig. 2C).

We tested the effect of pre-treating endothelium with the above agents on the route of lymphocyte migration. On rat brain MVECs, adrenomedullin and O-Me did not alter total adhesion or diapedesis (supplementary material Fig. S1D) and did not significantly alter the predominantly transcellular route usage (Fig. 2D). Histamine treatment, which minimally affected junctional integrity, also did not affect either total migration or the route used. However, PP2 treatment caused a significant (approximately twofold) increase in paracellular migration with a

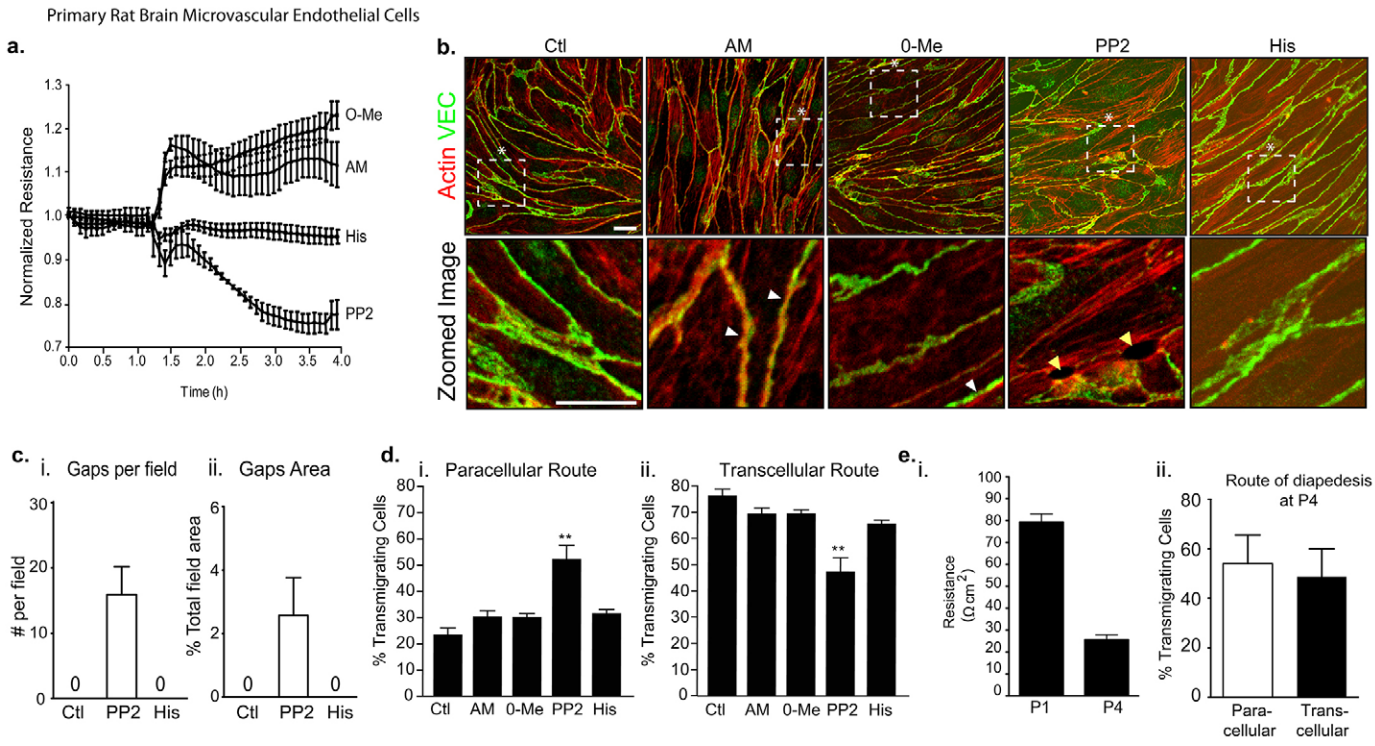

Fig. 2. Modulation of junctional integrity in rat brain MVECs affects the route of diapedesis. Primary rat brain MVECs were grown to confluence and stimulated with TNF-α (24 h) before the addition of adrenomedullin (AM, 10 μM), 8-pCPT-2′-O-Me-cAMP (O-Me, 200 μM), histamine (His, 300 μM) or PP2 (10 μM). (A) Changes in TEER are shown following treatments. Data show the mean±s.e.m. (at least four separate experiments). (B) Immunofluorescence imaging of rat brain MVECs following treatment with adrenomedullin and O-Me for 30 min and histamine or PP2 for 10 min prior to fixation, permeabilization and staining for VEC (green) and F-actin (red). The areas indicated by dashed boxes and asterisks are shown at higher magnification in the lower panels. Ctl, control; white arrowheads, cortical actin; yellow arrowheads, gaps. Data are representative of at least five separate experiments. Scale bars: 10 μm. (C) Quantification of the number of gaps per field (i) and the percentage of total gap area per field (ii) in PP2-treated and histamine-treated cells. (D) Rat brain MVECs were treated as before prior to the addition of rat T cells for 30 min followed by fixation, staining and quantification of paracellular (i) and transcellular diapedesis (ii). Data show the mean±s.e.m. (at least four separate experiments); $^{**}P<0.01$. (E) Comparison of basal TEER in primary rat brain MVECs at passage 1 (P1) and passage 4 (P4) (i) and quantification of the route of diapedesis at passage 4 (ii). Data show the mean±s.e.m. (at least three separate experiments).

Journal of Cell Science (2014) 127, 3720–3734 doi:10.1242/jcs.148619

concomitant decrease in transcellular migration (Fig. 2D). Importantly, PP2 and the above treatments did not change the expression of key adhesion molecules (e.g. ICAM1, VCAM1 and PECAM1; supplementary material Fig. S1F). This result suggests that alterations in junctional barrier properties can modify the route of leukocyte transmigration. As further confirmation for the role of 'junctional tightness' itself in the above results, we took advantage of an established agent-independent means of progressively reducing primary rat brain MVEC barrier strength through extended culture passaging (Lippmann et al., 2013). We found that by culturing rat brain MVECs for >4 passages, we could promote a substantial decrease in electrical resistance to ~26 Ωcm^2, which was coupled with a shift towards a majority of diapedesis occurring by the paracellular route (Fig. 2E).

We next investigated 'peripheral' endothelial cell types, known to have less-organized junctions and lower basal TEER compared with rat brain MVECs (Fig. 1A), and asked whether increasing barrier function to make them more 'brain-like' would lead to an increase in transcellular migration. To directly compare a different vascular bed in the same species, we investigated primary rat heart MVECs. As shown above, these cells exhibited lower TEER (~25 versus ~77 Ωcm^2; Fig. 1A) and a lower percentage of transcellular diapedesis compared with that of rat brain MVECs (~33% versus ~70%; Fig. 1D). In rat heart MVECs, adrenomedullin or O-Me promoted a significant increase in barrier function (Fig. 3A), which was coupled with increased cortical actin and more continuous and linear VEC staining (Fig. 3Ci). As predicted, pre-treatment with adrenomedullin or O-Me also significantly shifted diapedesis towards usage of the transcellular route (Fig. 3B, but without significant changes in total adhesion or diapedesis; supplementary material Fig. S1E). Alternatively, pre-treatment of rat heart MVECs with either histamine or PP2 reduced TEER (Fig. 3A) and induced stress fibers and VEC discontinuities (Fig. 3Ci–iii). This was coupled with an increased level of paracellular (Fig. 3B), but not total, adhesion or diapedesis (supplementary material Fig. S1E). Very similar endothelial responses and diapedesis route switching was found in human lung MVECs that were exposed to the above junction modifying agents (supplementary material Fig. S2). Importantly, this route switching occurred in the absence of significant changes in the expression or distribution of ICAM-1, VCAM-1 or PECAM-1 (supplementary material Fig. S1F; Fig. S3).

Changes in junctional integrity induced by fluid shear flow, altered substrate stiffness and genetic means promote diapedesis route switching

Exposure of endothelium *in vitro* to long-term (>12 h) steady-state laminar fluid shear flow promotes more physiologic and stable junctions with increased barrier function (Birukov et al.,

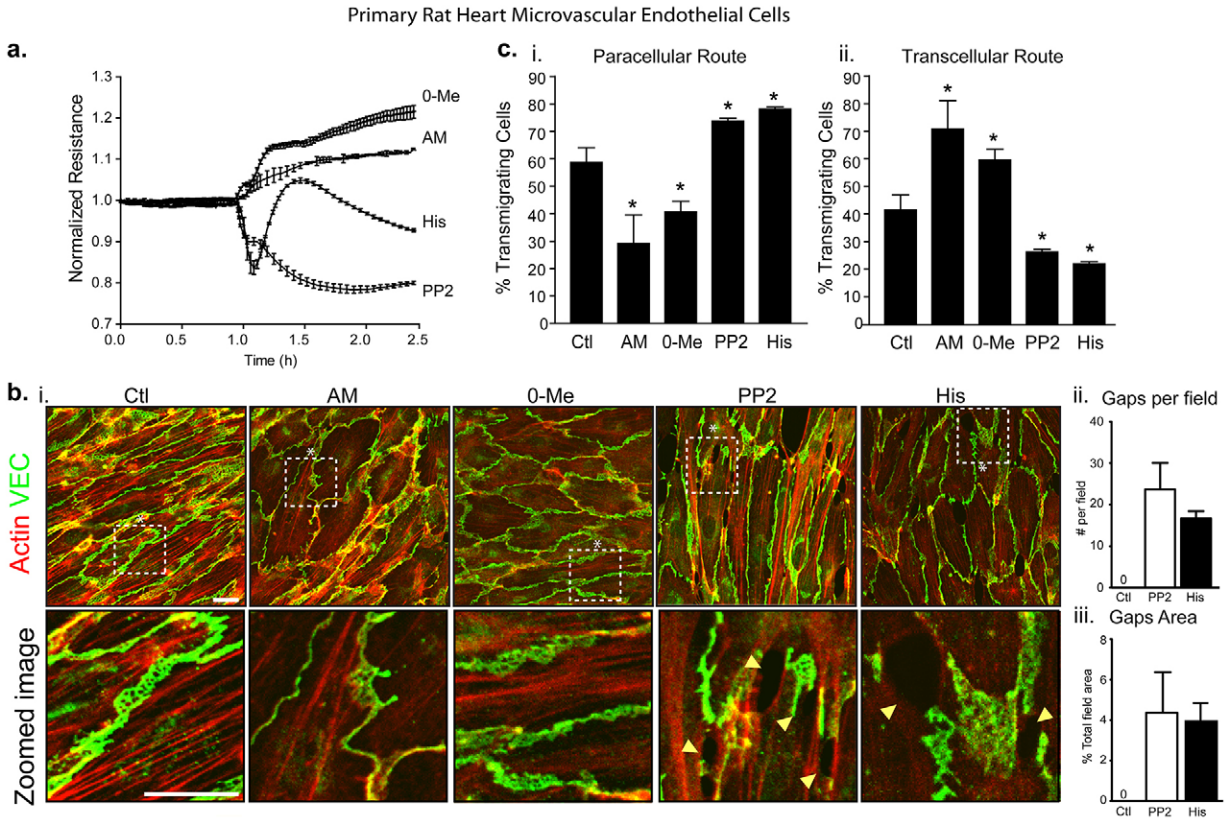

Fig. 3. Modulation of junctional integrity in rat heart MVECs affects the route of diapedesis. Primary rat heart MVECs were grown to confluence and stimulated with TNF-α (24 h) before the addition of adrenomedullin (AM, 10 μM), 8-pCPT-2′-O-Me-cAMP (O-Me, 200 μM), histamine (His, 300 μM) or PP2 (10 μM). (A) Changes in TEER are shown following treatments. Data show the mean±s.e.m. (at least four separate experiments). (B) Rat heart MVECs were treated as above prior to the addition of rat T cells for 10 min followed by fixation, staining and quantification of paracellular (i) and transcellular diapedesis (ii). Ctl, control. Data show the mean±s.e.m. (at least four separate experiments); *P<0.05. (C) Immunofluorescence imaging of rat heart MVECs following treatment with adrenomedullin and O-Me for 30 min and histamine or PP2 for 10 min prior to fixation, permeabilization and staining for VEC (green) and F-actin (red) (i) and quantification of the number of gaps per field (ii) and the percentage of total gap area per field (iii) in PP2-treated and histamine-treated cells (data show the mean±s.e.m.). In immunofluorescence images, the areas indicated by dashed boxes and asterisks are shown at higher magnification in the lower panels. Yellow arrowheads, gaps. Data are representative of at least five separate experiments. Scale bars: 10 μm.

Journal of Cell Science (2014) 127, 3720–3734 doi:10.1242/jcs.148619

2002). Here, we used shear conditioning to test our path-of-least-resistance hypothesis in a manner that was independent of hormones and pharmacological agents. A 48-h exposure of human lung MVECs to 10 dyne/cm^2 shear flow indeed resulted in more continuous junctions with strong cortical actin enrichment and a reduction in the amount of central stress fibers compared with that of non-sheared or acutely (30 min) sheared controls (Fig. 4A). To assess the functional consequences of these shear treatments on barrier properties, we implemented a quantitative imaging-based fluorescent tracer permeability assay (Dubrovskyi et al., 2013). This revealed that long-term, but not short-term, shear significantly decreased basal permeability and increased junctional barrier function (Fig. 4Aii,iii). Parallel permeability studies using human lung MVECs treated with either

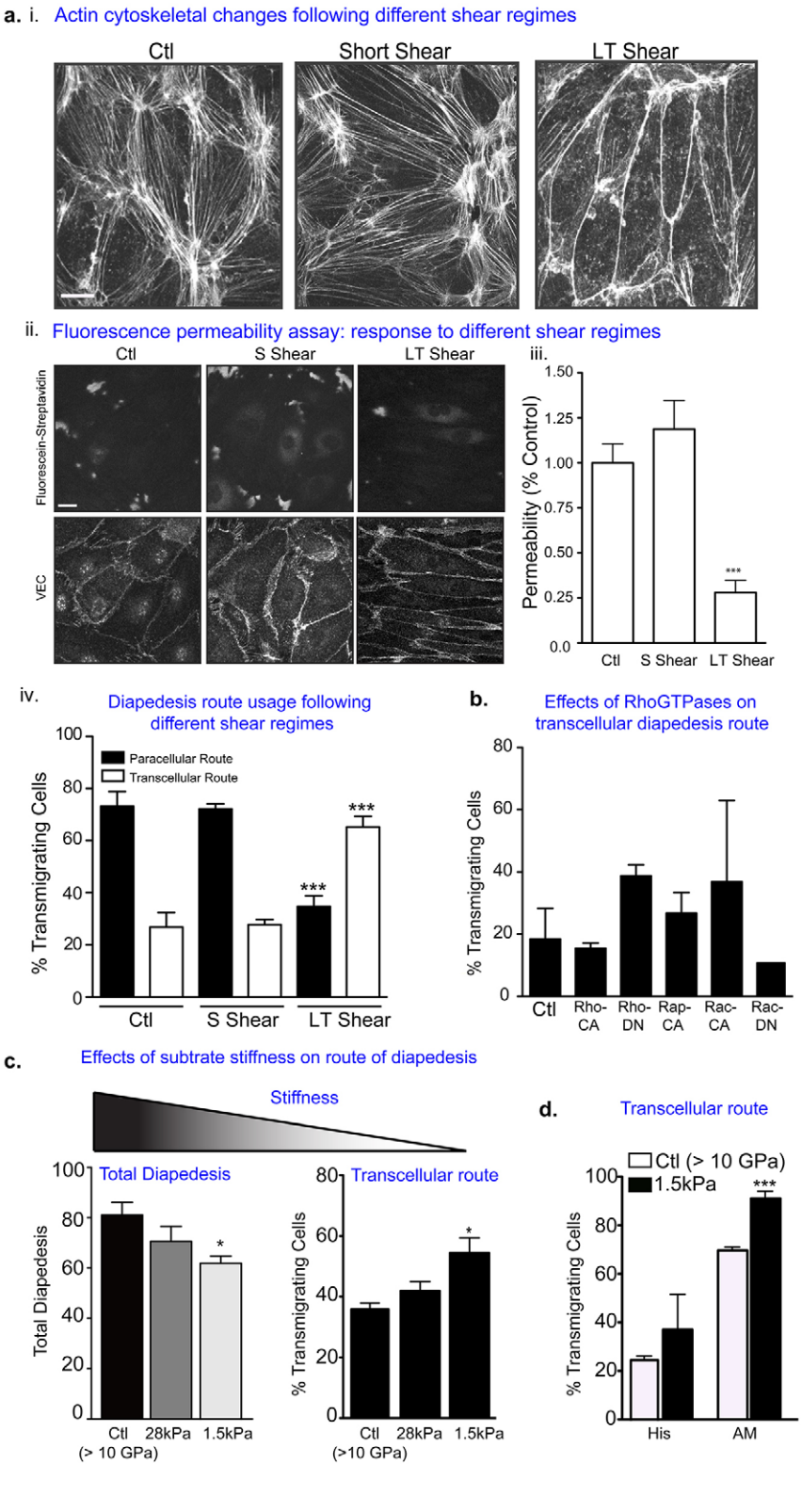

Fig. 4. Effect of shear flow, genetic modulation of Rho GTPases and substrate stiffness on route of migration. (A) Human lung MVECs were grown to confluence, stimulated with TNF-α (24 h) and exposed to short (S) or long-term (LT) shear (30 min or >36 h, respectively; 10 dyne/cm^2). (i) Samples were fixed and stained for actin, or subjected to fluorescent tracer permeability (ii, iii) or diapedesis (iv) assays. (ii) Representative images of paracellular 'leakage' of fluorescein–streptavidin that was 'captured' on the biotin-coated substrate underlying the endothelium (upper panels) near VEC-stained junctions (lower panels). Scale bars: 10 μm. (iii) Quantification of the permeability under static (control, Ctl), short or long-term shear conditions. (iv) Human T cells were added for 10 min to allow for migration, followed by fixation, staining and quantification of total diapedesis (see supplementary material Fig. S4Aii) and route of diapedesis. (B) Human lung MVECs were transfected with constitutively active (CA) Rho, Rap or Rac or dominant negative (DN) Rho or Rac, followed by fixation, staining and quantification of the route of diapedesis. (C) Human lung MVECs were grown to confluence on either glass (>10 GPa) or elastic substrates of 28 kPa and 1.5 kPa elastic modulus. Cells were stimulated with TNF-α (24 h) before the addition of human T cells for 10 min followed by fixation, staining and quantification of total diapedesis (left) and transcellular route usage (right). (D) Human lung MVEC monolayers were prepared as above on glass (>10 GPa; control; white bars) or an elastic substrate (1.5 kPa; black bars) and then treated with adrenomedullin (AM, 10 μM) or histamine (His, 300 μM) before the addition of human T cells for 10 min and quantification of the route of diapedesis. Quantitative data show the mean±s.e.m. [at least four (A,C,D) or three (B) separate experiments]; *P<0.05, ***P<0.001.

adrenomedullin or histamine (supplementary material Fig. S4B) demonstrate that the fluorescent tracer assay produces estimates of endothelial cell barrier function that, qualitatively, agree well with our TEER-based measurements (e.g. supplementary material Fig. S2C). Following exposure to static, acute or long-term shear pre-conditioning, all diapedesis was allowed to proceed under the same static conditions, as the effect of shear persists for $\geq$10 min after the cells are returned to static conditions (supplementary material Fig. S4Ai). Consistent with our hypothesis, cytoskeletal rearrangements and barrier strengthening induced by long-term shear conditioning promoted significantly greater transcellular diapedesis (Fig. 4Aiv), which, in this setting, was not associated with significant alterations in total diapedesis (supplementary material Fig. S4Aii).

Next, we promoted alterations in cytoskeleton and junctional integrity through a genetic approach (Spindler et al., 2010; Wojciak-Stothard and Ridley, 2002). Transfection of human lung MVECs with constitutively active (CA)-RhoA or dominant negative (DN)-Rac1, which promote the formation of stress fibers and paracellular gaps, tended to reduce the occurrence of transcellular diapedesis in favor of paracellular diapedesis (Fig. 4B). Alternatively, DN-RhoA, CA-Rap1 and CA-Rac1, which promote cortical actin, stimulated greater transcellular diapedesis (Fig. 4B).

Extensive emerging studies have demonstrated that Rho-GTPase signaling, cytoskeletal organization, contractility and cell stiffness are all responsive to the mechanical properties (i.e. stiffness, elasticity) of the substrate (Discher et al., 2005; Tee et al., 2009). As we and others have shown, growing endothelial cells on softer, more physiologic, elastic substrates promotes a reduction in overall contractility and stiffness, stress fibers, Rho signaling and paracellular gaps and permeability (Krishnan et al., 2011). Typical cell culture plastic or glass dishes have stiffnesses >10 gigaPa (GPa). Physiologic substrates range from ~1 to ~90 kiloPa (kPa). However, increases in cell stiffness are only seen over the limited range of substrate stiffnesses of ~1 to 10 kPa, after which the cell stiffness reaches a maximum that is similar to that of a cell on glass or plastic (Tee et al., 2009). Thus, in these studies, we compared cells cultured on two relatively stiff substrates [i.e. glass and polymethylsiloxane (PDMS) with an elastic modulus of 28 kPa] and one relatively 'soft' substrate (i.e. 1.5-kPa PDMS). These studies showed that the soft substrate promoted significantly more transcellular diapedesis (Fig. 4C) that was associated with greater amounts of cortical actin versus stress fibers, as well as a modest reduction in total diapedesis (Fig. 4C; supplementary material Fig. S4C). Furthermore, the relative fraction of transcellular diapedesis that occurred following either treatment with histamine or adrenomedullin was greater was on soft 1.5-kDa substrates compared with glass (Fig. 4D). These findings demonstrate that manipulation of the endothelial cell cytoskeleton and mechanical properties through defined substrate stiffness can alter route utilization. Additionally, these observations, together with those made above using physiologic shear, suggest that paracellular diapedesis might be overrepresented in common *in vitro* models.

Lymphocytes probe the endothelium physically during lateral migration

Our results thus far establish that coordinated modulation of the junctional strength and the balance between cortical actin and actin stress fibers crucially influence the route of lymphocyte diapedesis. But how do the lymphocytes perceive or experience these changes? It is established that as leukocytes laterally migrate on endothelia they dynamically extend exploratory lamellipodia and pseudopods (Ley et al., 2007; von Andrian and Mackay, 2000). We and others recently demonstrated that they also extend and retract invadosome/podosome-like protrusions (ILP) that physically push against the endothelial cell surface and junctions (Carman, 2009; Carman et al., 2007; Gérard et al., 2009; Lyck and Engelhardt, 2012; Shulman et al., 2009). Electron microscopy in the current study provides orthogonal views of such spherically tipped (~400–800-nm diameter) cylindrical ILPs sharply indenting the human lung MVEC plasma membrane at junctional and non-junctional regions of the endothelial cell body (Fig. 5A,B). Additional live-cell fluorescence microscopy provided 'en face' imaging of highly dynamic and avid cytosol-displacing ILPs probing at and away from cell junctions during lateral migration (Fig. 5C; supplementary material Movie 1). Similar behaviors were seen on rat brain MVECs (supplementary material Fig. S4C).

ILPs might function in local sampling of endothelial stiffness

We hypothesized that ILPs could provide a mechanism for local sampling of mechanical properties (e.g. stiffness and junctional adhesive strength) of the endothelial barrier. To test this idea, we designed an approach to directly 'feel' the endothelium in a manner analogous to lymphocyte ILPs. Specifically, we employed atomic force microscopy (AFM)-enabled nanoindentation (Lee et al., 2010) coupled to a 600-nm diameter spherically tipped cantilevered probe that approximates ILP geometry (Carman, 2009) (Fig. 6A). In this way, we measured changes in stiffness at the junction in response to agents that alter junctional integrity and F-actin, a major determinant of cell stiffness (Pesen and Hoh, 2005; Rotsch and Radmacher, 2000; Wakatsuki et al., 2001). We found that agents that promote junctional strengthening and cortical F-actin and reduce paracellular diapedesis (i.e. adrenomedullin and O-Me) tended to increase junctional stiffness (Fig. 6Bi–iii,C). Conversely, histamine and PP2, which promote loss of cortical actin in favor of central stress fibers and increase paracellular diapedesis, decreased stiffness at the junctions (Fig. 6Biv,v,C). These results are highly consistent with a previous study that coordinately assessed barrier function, actin remodeling and local cell stiffness (but not diapedesis) in endothelium in response to related barrier-modifying stimuli (Birukova et al., 2009). These experiments suggest that barrier-altering regimes promote changes in junctional stiffness that ILPs would identify.

Inverse correlation between nuclear localization, F-actin density and subcellular zones of diapedesis

The above results imply that relative local F-actin density, and the biomechanical stiffness it imparts, might play important (though not necessarily exclusive) roles in determining the route and sites of diapedesis. Indeed, F-actin is known to be one of the primary determinants of cellular stiffness in most cell types (Pesen and Hoh, 2005; Rotsch and Radmacher, 2000; Wakatsuki et al., 2001), second only to the nuclear lamina (typically ~5–10-fold stiffer than F-actin structures; Caille et al., 2002; Dahl et al., 2010; Dahl et al., 2008). Thus, we postulated that specific subcellular loci for diapedesis would exclude the endothelial nucleus and, in non-nuclear regions, correlate inversely with F-actin distribution in endothelial cells.

Our extensive ultrastuctural studies demonstrated that lymphocytes positioned over the endothelial nucleus avidly protruded ILPs that apparently supplied enough force to deform, but never breach nuclear lamina (Fig. 7A). In some

Journal of Cell Science (2014) 127, 3720–3734 doi:10.1242/jcs.148619

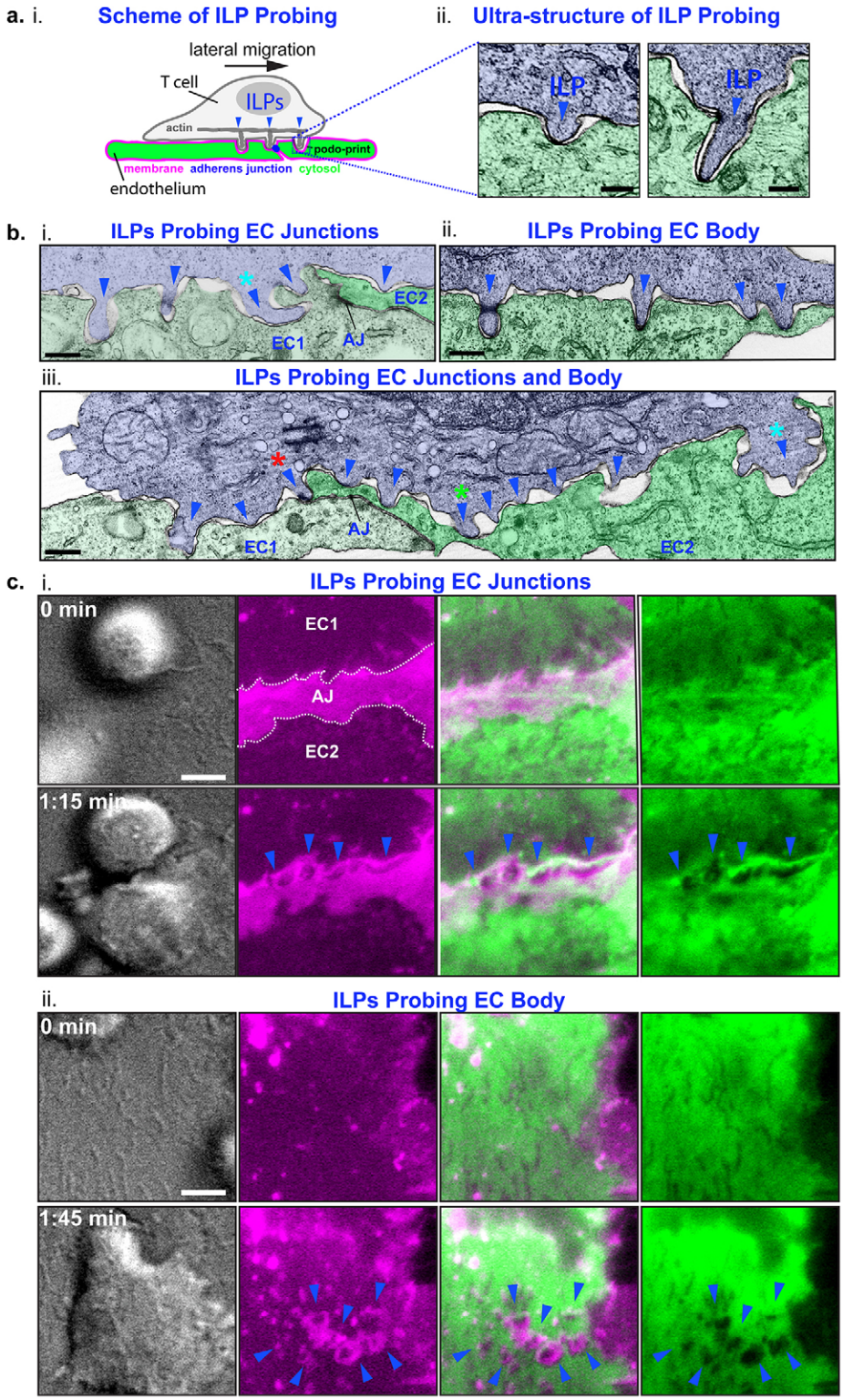

Fig. 5. Lymphocytes 'feel' the vascular endothelium through invadosome-like protrusions. (A) (i) Orthogonal schematic view of a lymphocyte forming invadosome-like protrusions (ILPs) against the endothelial surface. (ii) Representative ultrastructural views of primary lymphocyte (blue) ILP (blue arrowhead) deforming the surface of activated endothelium (green). Scale bars: 300 nm. (B) Examples of ILPs (blue arrowheads) probing the junctions and endothelial cell (EC) body. (i) Note two separate ILPs on either side of an adherens junction (AJ) and one 'burrowing' ILP or pseudopod (cyan asterisk). (iii) Note one ILP protruding at the adherens junction (red asterisk) and one protruding at an adjacent highly tenuous non-junctional region (green asterisk), as well as a burrowing ILP (cyan asterisk). Data are representative of >100 images. Scale bars: 500 nm. (C) Human lung MVECs were transfected with MemDsRed (magenta) and soluble GFP (green; a cytoplasm volumetric marker), stimulated with TNF-α (24 h) and subjected to live-cell imaging in the presence of T cells. Upper panels show a time-point shortly after lymphocytes have settled on the endothelium, but before the formation of ILPs (relative time=0 min). Lower panels show a time-point after lymphocyte spreading and formation of ILPs (relative time 1.15 or 1.45 min). Note that for each MemDsRed ring, a circular region of diminished GFP signal is formed, indicating cytoplasm displacement by ILPs (blue arrowheads). These can be seen pushing into the MVEC at the cell–cell junctions (i) or in the cell body (ii). See also corresponding supplementary material Movie 1. Data are representative of >50 separate experiments. Scale bars: 5 μm.

such cases, a single T cell could be seen concomitantly protruding shallow ILPs against the nucleus and deeper cell-penetrating ILPs at sites immediately adjacent to it (Fig. 7Aiii). In live-cell imaging studies, we confirmed that lymphocytes dynamically protruded ILPs against the nuclear lamina as they laterally migrated over it (Fig. 7B; supplementary material Movie 2). Yet, perhaps not surprisingly, in >200 separate dynamic imaging experiments (as well as extensive fixed end-point imaging experiments), lymphocytes were never seen to transmigrate directly through the endothelial nucleus. However, as also shown above by electron microscopy, they occasionally transmigrated at sites close to the nucleus (Fig. 7B, yellow arrowhead; supplementary material Movie 2). These data support the simple idea that local levels of endothelial stiffness can crucially affect sites of diapedesis. Additionally, they suggest that ILP protrusive strength must fall below, but in the general range

Journal of Cell Science (2014) 127, 3720–3734 doi:10.1242/jcs.148619

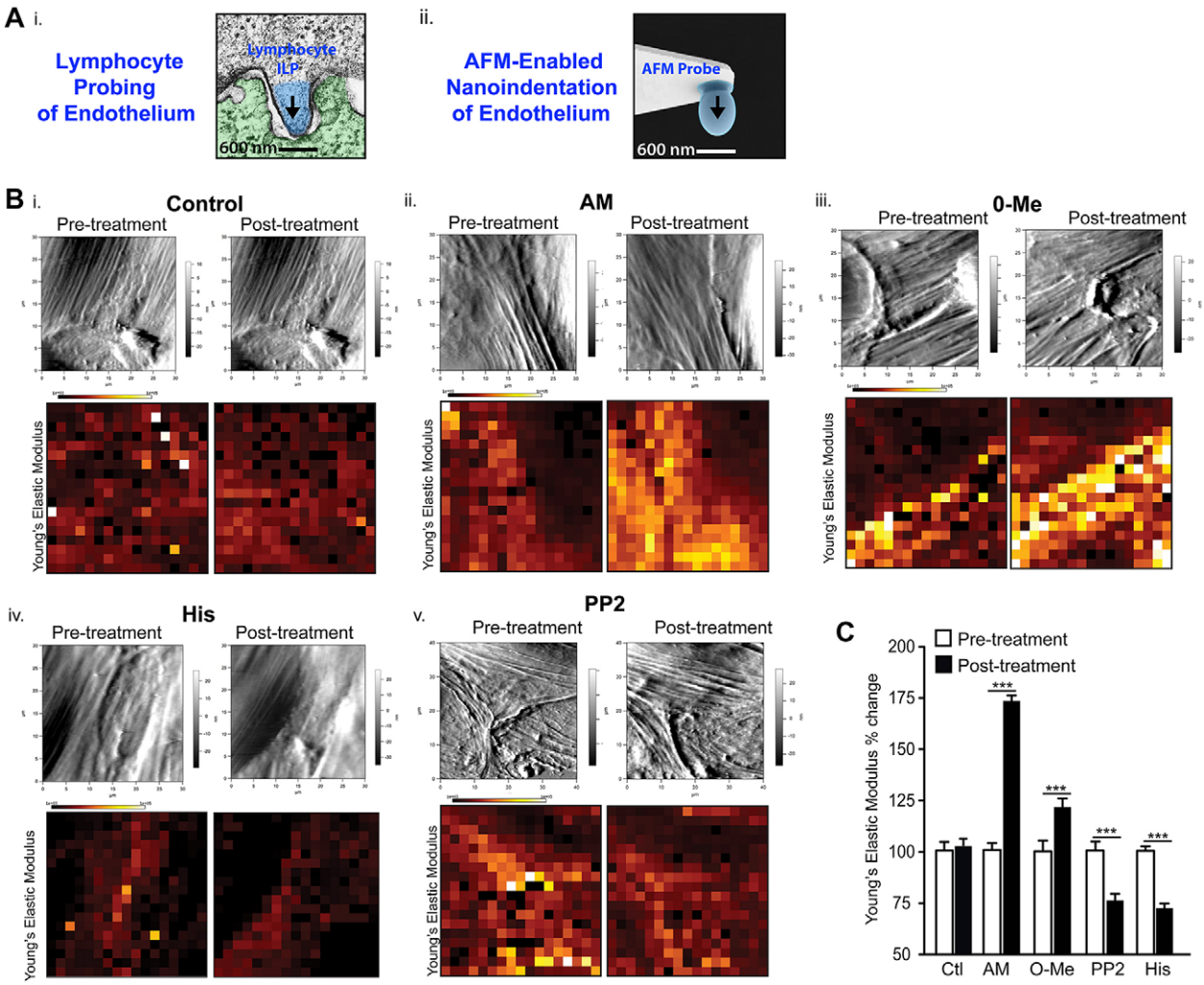

Fig. 6. AFM-enabled nanoindentation to assess the stiffness of endothelial junctions. (A) Comparison between the size and shape of a single ILP (i) and the AFM probe used (ii). (B) Representative AFM height (upper panels) and corresponding Young's Elastic Modulus (lower panels) micrographs taken at the junction of human lung MVECs before and after the indicated treatments. (C) Quantification of the percentage change in Young's Elastic Modulus. Data show the mean±s.e.m. (at least four separate experiments); ***$P<0.001$.

of the endothelial cell nuclear stiffness, which is ~8 kPa (Caille et al., 2002). This is consistent with measurements made for several types of actin polymerization that show stalling of protrusions against stiffness in the range of ~1 to several kPa (Ludwig et al., 2008).

Compared with the nuclear regions, cell stiffnesses in non-nuclear areas fall under a lower and broader range (~0.2–3 kPa), which is largely governed by F-actin density, (Pesen and Hoh, 2005; Rotsch and Radmacher, 2000; Wakatsuki et al., 2001; Wang and Sun, 2012). To test the hypothesis that diapedesis sites might correlate inversely with local F-actin density and stiffness (which varies greatly within individual cells), we first carried out dynamic imaging to assess the density of actin–GFP at sites where T cells transmigrated, relative to the averaged actin–GFP density across the entire cell area. Studies were performed either by adding few T cells and tracking them individually until diapedesis was initiated (Fig. 7Ci) or by completely covering the endothelium with T cells and assessing the sites of T-cell-mediated endothelial breach after a fixed duration (Fig. 7Cii,iii). In both cases, preferred diapedesis locations were consistently those of relatively lower F-actin density (i.e. ~50% lower versus total averaged density). No such bias was identified with respect to the density of microtubules or vimentin intermediate filaments (Fig. 7Ci,ii), which is in agreement with previous studies demonstrating a dominant contribution of the actin cytoskeleton in determining the stiffness of endothelial cells (Pesen and Hoh, 2005; Rotsch and Radmacher, 2000; Wakatsuki et al., 2001).

Detailed study of our dynamic imaging experiments revealed several important findings. First, although the role of lateral migration has often been posited to be simply a means of getting leukocytes to the junctions to allow for paracellular diapedesis, we frequently observed T cells laterally migrating over and past junctions, while avidly palpating but not breaching them (supplementary material Movie 3; see also Fig. 5Bi,iii). These cells often went on to undergo diapedesis at distinct paracellular or transcellular sites. We also observed many T cells that migrated laterally, never encountered a junction and ultimately migrated transcellularly (see examples below).

Second, at zones of extremely dense endothelial actin meshwork or stress fibers, T cells exhibited avid 'frustrated' ILP probing without breaching of the endothelium (i.e. similar to the behavior seen over the nucleus) (Fig. 8Ai; supplementary

Journal of Cell Science (2014) 127, 3720–3734 doi:10.1242/jcs.148619

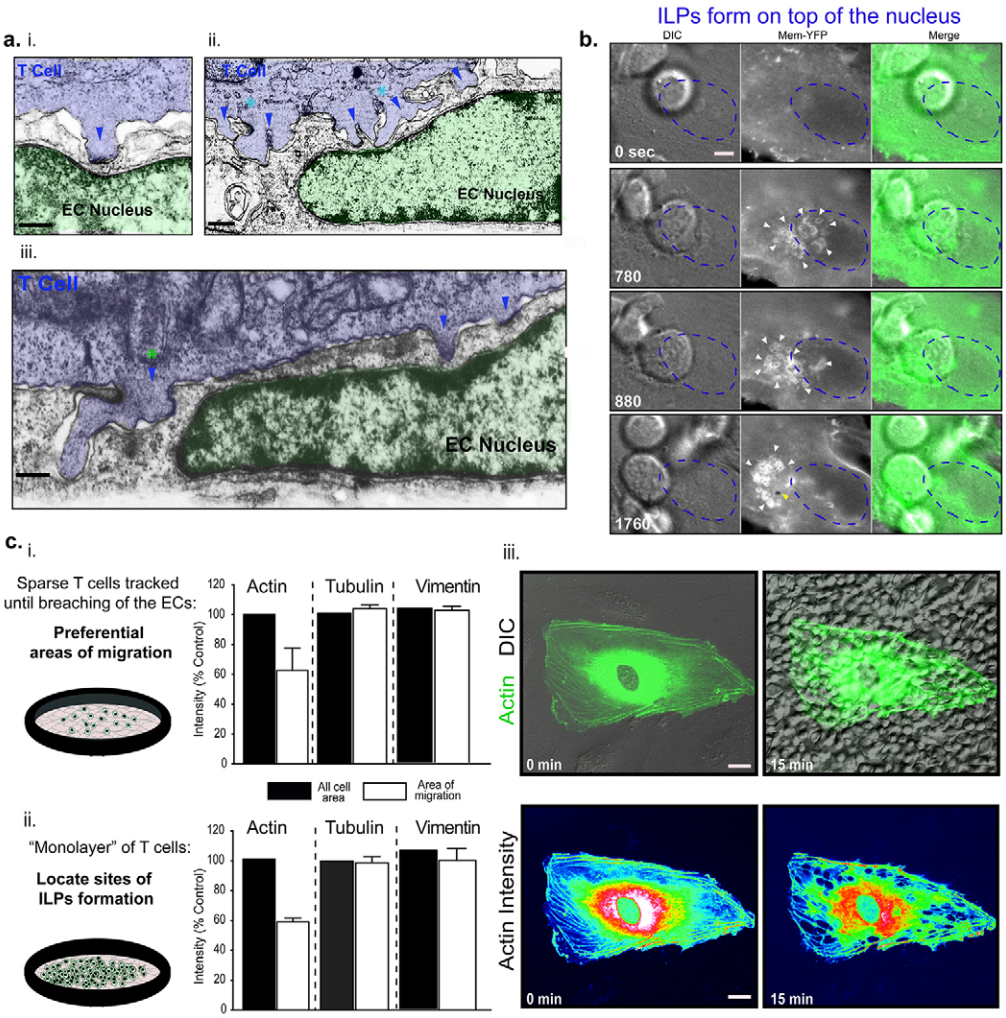

Fig. 7. Assessing the contribution of endothelial nuclear lamina and cytoskeleton in determining sites of lymphocyte diapedesis. (A) Electron microscopy micrographs of lymphocyte ILPs (blue arrowheads) formed above the endothelial cell (EC) nuclei (green). Note that individual (i) or clustered ILPs (ii) (and burrowing ILPs or pseudopods; cyan asterisks) can be seen exerting sufficient force to locally deform the nuclear lamina. (iii) Example of concomitant formation of both shallow 'frustrated' ILPs above the nucleus (blue arrowheads) and a deeply cytoplasm-penetrating ILP immediately adjacent to the nucleus (green asterisk). Scale bars: 500 nm. (B) Live-cell imaging showing a T cell avidly probing with multiple ILPs (white arrowheads) in the area above the endothelial cell nucleus (dashed blue line) before forming a transcellular pore adjacent to the nucleus. DIC, differential interference contrast. Scale bar: 5 μm. See also corresponding supplementary material Movie 2. (C) Human lung MVECs were transfected with MemDsRed and either actin–GFP, tubulin–GFP or vimentin–GFP, stimulated with TNF-α (24 h) and subjected to live-cell imaging during T cell diapedesis. The density of actin, tubulin and vimentin at the sites of barrier breach were quantified as described in Material and Methods. (i) Experiment type 1: a low density of T cells was added to the MVEC monolayer and each individual lymphocyte was tracked until the initiation of diapedesis. (ii) Experiment type 2: a high (saturating) density of T cells was added to the MVEC monolayer and all sites of diapedesis initiation were identified at a fixed time-point of 15 min. Data show the mean±s.e.m. (at least seven separate experiments). (iii) Representative images of experiment type 2: upper panels show merged DIC and fluorescence images of a singular actin–GFP-transfected human lung MVEC in the context of a confluent monolayer at time 0 and 15 min after addition of T cells. Lower panels show the corresponding fluorescence intensity heat maps of actin distribution. Data are representative of at least seven separate experiments. Scale bars: 10 μm.

material Movie 4, 'cell 1'). Additionally, when T cells did occasionally manage to initiate a breach in regions of dense F-actin, the pore typically took on an elongated slit shape that seemed to be dictated by the architecture of the endothelial actin filaments. In such cases, the T cells seem unable to sufficiently deform the dense filaments and expand a diapedesis passageway, leading to failed and aborted transmigration attempts (Fig. 8Ai; supplementary material Movie 4, 'cell 2'). In cells or regions with modest actin density, ILP probing could be more clearly seen to cause bending and distortion of individual endothelial actin filaments or small filament bundles during lateral migration (Fig. 8B; supplementary material Movie 5). Successful barrier breaching and diapedesis could ultimately be seen as the lymphocytes reached zones of relatively reduced F-actin density (Fig. 8B; supplementary material Movie 5). At zones with low F-actin density, T cells exhibited seemingly unimpeded breaching of the endothelium by extending ILPs into the space between two or more actin filaments, which subsequently were readily distorted and 'bowed out' to accommodate the completion of diapedesis (Fig. 8Aii; supplementary material Movie 6). Correlated ultrastructural studies also evidenced 'frustrated' ILPs protruding against thick endothelial F-actin bundles that showed little deformation and more deeply 'borrowing' ILPs that were readily seen to push against, distort and bow out more sparse filaments (Fig. 8C).

Journal of Cell Science (2014) 127, 3720–3734 doi:10.1242/jcs.148619

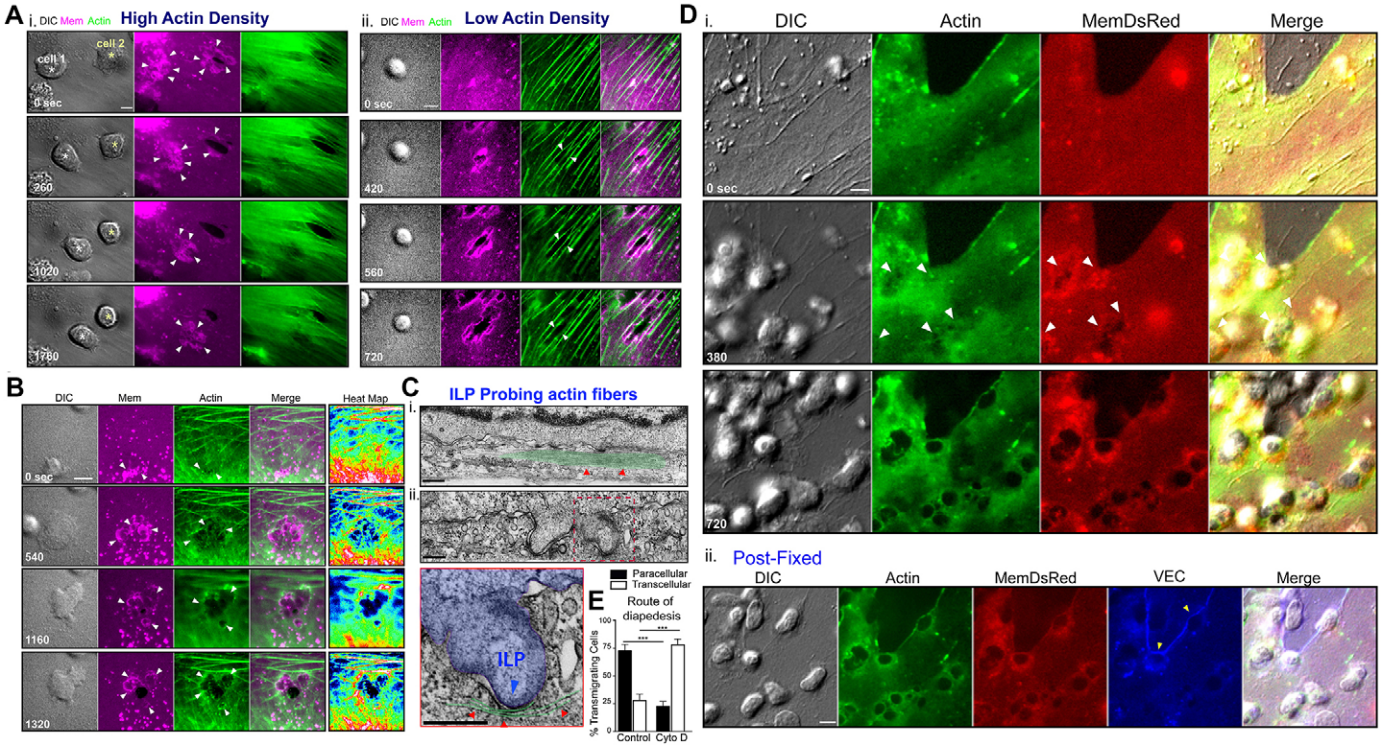

Fig. 8. Tenertaxis: lymphocytes actively probe the endothelial cell surface and underlying cytoskeleton and prefer to migrate in areas of low F-actin. (A) Human lung MVECs were transfected with actin–GFP (green) and MemDsRed (magenta) and stimulated with TNF-α (24 h) before the addition of T cells and live-cell imaging. (i) In areas of high-density actin filaments, T cells are seen to avidly palpate the MVEC with numerous frustrated ILPs (arrowheads) without initiation of diapedesis (cell 1). Alternatively, T cells that initiate breach in areas of dense actin are often unable to complete diapedesis (cell 2). See also corresponding supplementary material Movie 4. (ii) In areas of lower actin density, ILP can be seen readily driving barrier breach between actin fibers. See also corresponding supplementary material Movie 6. DIC, differential interference contrast. (B) In areas of modest actin density, ILPs can be seen to dynamically bend the actin fibers (white arrowheads) during lateral migration, which ultimately allows for diapedesis upon reaching a region of relatively lower actin density (see heat map panels). See also corresponding supplementary material Movie 5. (C) (i) Representative electron microscopy micrograph of frustrated ILPs failing to deform thick F-actin bundles (green). Red arrowheads, actin filaments. (ii) Representative electron microscopy micrograph of ILPs readily bending or distorting individual actin filaments. The area outlined in red is shown at higher magnification in the lower image. (D) (i) Human lung MVECs were transfected with actin–GFP (green) and MemDsRed (red), stimulated with TNF-α (24 h) and treated with cytochalasin D (200 mM, 30 min at 37°C) before the addition of T cells and live-cell imaging. (ii) Following 10–15 min of imaging, samples were fixed and stained for VEC (blue) to identify the adherens junctions. ILP probing (white arrowheads) can be seen to readily form transcellular breaches throughout the cell body (i), as well as adjacent to intact VEC junctions (ii, yellow arrowheads). See also corresponding supplementary material Movie 7. Scale bars: 5 μm (for A,B,D), 200 nm (for C). (E) Quantification of the route of migration following cytochalasin D treatment. Data show the mean±s.e.m. (at least five separate experiments); ***$P<0.001$.

Taken together, these observations suggest that dense F-actin (whether cortical actin at the junctions or actin bundles, meshwork or stress fibers in the center of the cell) provides a strong physical barrier to diapedesis. As a further test of this possibility, we examined the effect on T cell diapedesis of pharmacologic depolymerization of total endothelial F-actin by treatment with cytochalasin D (a regime known to dramatically lower cellular stiffness; Pesen and Hoh, 2005; Rotsch and Radmacher, 2000; Wakatsuki et al., 2001). In the context of confluent endothelial monolayers with preformed adherens junctions, we found that although a 30-min treatment with cytochalasin D caused a profound depletion of actin filaments throughout the cell, significant amounts of dense cortical actin remained intact at (and apparently stabilized by) the cell junctions (supplementary material Fig. S4D). In diapedesis experiments, we found that the lymphocytes readily formed transcellular pores in the endothelium throughout the F-actin-depleted cell body (with the exception of the nuclear region) (Fig. 8D,E; supplementary material Movie 7). Importantly, although many T cells migrated transcellularly in close contact to VE-cadherin-positive intact junctions (Fig. 8Dii), relatively little migration occurred through the junctions (Fig. 8E). Thus, the overall tendency of the lymphocytes was to undergo diapedesis in what can reasonably be inferred, based on the level of F-actin, to be the zones of lowest endothelial cell stiffness.

DISCUSSION

Our studies show that lymphocytes can switch their diapedesis route preference in settings of differing inter-endothelial adhesive strength (which is coordinated with alterations in the balance between cortical actin and stress fibers). Importantly, although endothelial adhesion molecules are essential for diapedesis in general, the observed route switching could not be attributed to changes in their levels or distribution. Moreover, we find that dynamic ILP probing by lymphocytes allows them to efficiently test the local mechanical strength or stiffness of the endothelial barrier during lateral migration. This facilitates the identification of sufficiently tenuous sites on the endothelium for the initiation of paracellular or transcellular breaches. We term this path-of-least-resistance-seeking behavior ‘tenertaxis’ (from the Latin, *tener* – soft, tender, tenuous). Although this study was conducted in a model of inflammation, we expect that these findings will

Journal of Cell Science (2014) 127, 3720–3734 doi:10.1242/jcs.148619

likely hold true for diapedesis during hematopoiesis, homing and general surveillance. These results have important implications for understanding (i) the relationship between leukocyte diapedesis and overall vascular endothelial barrier regulation and (ii) the role of substrate mechanics in migration biology.

Relevance and role of two routes of diapedesis

The ability to seek out both junctional and non-junctional sites for barrier breach means that as endothelia increase their overall junctional strength and barrier function (i.e. with respect to fluid and solutes) the net result might be a tendency towards switching of route, rather than necessarily an abrogation of diapedesis. Importantly, *in vivo*, different contexts (e.g. distinct vascular beds and differing constitutive or inflammatory conditions) support broadly ranging route usage from essentially totally transcellular to almost completely paracellular diapedesis (Carman, 2009; Sage and Carman, 2009). Although lacking direct assessment of migration routes, a range of *in vivo* and *in vitro* studies support this idea. For example, engineered approaches to stabilize the VE-cadherin–actin association at adherens junctions and thereby 'lock' closed the adherens junctions *in vivo* only partially reduce diapedesis in inflammatory settings, but have no effect on the extensive constitutive trafficking events (e.g. hematopoiesis, homing, etc) (Vestweber, 2012). Similarly, sealing of the blood–brain-barrier tight junctions by ectopic expression of claudin-1 in a murine model of multiple sclerosis significantly reduces plasma leak and ameliorates disease, but does not alter immune cell trafficking (Pfeiffer et al., 2011). Adrenomedullin-2 treatment strongly stabilizes endothelial junctions and blocks leakage of plasma, but not leukocyte infiltration, in a model of lung injury (Müller-Redetzky et al., 2012). Finally, O-Me treatment of HUVECs *in vitro* enhances junctional integrity and cortical actin, which strongly blocks egress of solute but not neutrophils, leading the authors to suggest that these processes might be independently regulated (Cullere et al., 2005). In agreement with the above findings, our studies herein show that, under pro-migratory conditions (i.e. TNF-α activation of MVECs), tighter junctions had variable effects on total diapedesis efficiency ranging from a modest decrease (e.g. brain MVECs versus peripheral MVECs or culture on 1.5-kPa soft substrates versus stiff substrates) to no detectable effects. Yet, in all cases, tighter junctions were associated with rerouting towards greater relative transcellular route usage. Conversely, incremental loosening of junctions favored paracellular migration generally without increasing total diapedesis, although we would certainly predict that gross scale pathologic disruption of endothelial junctions would promote elevation of leukocyte trafficking.

Among all of the functions of the vascular endothelium, perhaps its most essential is the partitioning of the blood and tissue and the maintenance of a homeostatic balance of fluid and extracellular protein (Dudek and Garcia, 2001; Mehta and Malik, 2006). This function depends on the strength and remodeling of the junctions to meet the specific needs of each tissue as they vary in time and space. By contrast, immune cells have the crucial need to perform surveillance of tissues and respond to infection, which requires breaching the endothelial barrier. The transcellular mode of diapedesis might function to assist the co-existence of these two essential, but sometimes opposing functions. Said another way, if paracellular diapedesis was the only way for leukocytes to migrate, then the regulation of fundamental functions of the immune system would be forced into lockstep with the regulation of basic physiological functions of modulating fluid and solute equilibrium in tissues. Thus, the existence of two routes for leukocyte trafficking across the endothelium could be viewed as a compromise between the often contradictory functions of tissue and barrier cells and inherently invasive immune cells. An interesting further example of this is seen in the gut epithelium, where dendritic cells must conduct immune surveillance by sampling of the luminal bacterial flora. Here, rather than contend with (or risk perturbing) the extremely stable adherens and tight junctions, the dendritic cells pierce this barrier transcellularly (through the use of structures highly reminiscent of the ILPs described herein) at specific regions of attenuation (i.e. M-cells), presumably the path of least resistance in this setting (Lelouard et al., 2012).

Our findings here might have important practical implications. They suggest that anti-inflammatory therapies aimed at blocking leukocyte trafficking through promoting junctional-integrity might not be particularly effective and that we rather should continue to focus on preventing the initial leukocyte–endothelial interactions. An interesting corollary is that, in settings such as sepsis, the desirable goal of strengthening junctions to reduce leak might be achieved without compromising effective leukocyte trafficking and bacterial clearance.

Tenertaxis – probing for barrier weak spots

Despite being an active player in diapedesis, the endothelium is also a physical barrier. The current study was designed in part to address the hypothesis that biomechanical features of this barrier might represent important determinants of diapedesis route or location. Implicit in this hypothesis is the idea that i) local heterogeneity exists in endothelial biomechanics and that this might be altered in time and space (e.g. in accordance with route switching) and ii) that leukocytes are somehow equipped to sense or feel these features.

Perhaps the most important biomechanical features of the endothelial barrier are the junctional strength and the cellular stiffness, both of which are crucially influenced by the actin cytoskeleton (Dudek and Garcia, 2001; Mehta and Malik, 2006; Pesen and Hoh, 2005; Rotsch and Radmacher, 2000; Wakatsuki et al., 2001). As many studies have evidenced, we find that junctional strength and integrity varies dramatically, dynamically and locally as assessed by TEER measurements and confocal imaging. We also find that junctional strength correlates with the amount of cortical actin and junctional stiffness. In non-junctional areas, significant and dynamic stiffness heterogeneity within individual endothelial cells is generated by the position of nucleus (Caille et al., 2002; Dahl et al., 2010; Dahl et al., 2008) and local density gradients of F-actin (Pesen and Hoh, 2005; Rotsch and Radmacher, 2000; Wakatsuki et al., 2001). Although microtubules to some degree and certainly intermediate filaments contribute to cell stiffness (e.g. Seltmann et al., 2013), in the endothelium these contributions seem to be secondary to those of actin microfilaments (Fels et al., 2014). Our results show that lymphocytes never transmigrate through the highly stiff nucleus and that, in non-nuclear areas, diapedesis efficiency is inversely correlated with F-actin density and stiffness. So how do the leukocytes 'feel' these biomechanical features?

It is well established that leukocytes dynamically extend exploratory F-actin-rich protrusions that can both exert and sense forces. For example, leading edge lamellipodia probe the external environment and alter dynamics to flow around rigid obstacles (Weiner et al., 2007). Furthermore, we and others have shown

that leukocytes project and retract ILPs into the cell surface and junctions during their lateral migration over the endothelium *in vitro* and *in vivo*, and that this process precedes, and is required for, efficient diapedesis (Carman, 2009; Carman et al., 2007; Gérard et al., 2009; Lyck and Engelhardt, 2012; Shulman et al., 2009). Our studies using AFM-enabled nanoindentation with an ILP-scaled probe suggest that T cell ILPs would experience changes in stiffness induced by barrier-altering stimuli. Although our studies do not assess whether T cell ILPs can serve as formal stiffness 'mechanosensors', invadosomes in other cell types have been shown to function as dynamic mechanosensors that sense and respond differentially to matrices of varied stiffness (Albiges-Rizo et al., 2009; Alexander et al., 2008; Collin et al., 2008). Dynamic and ultra-structural imaging demonstrated that whereas ILPs were 'frustrated' when they encountered nuclear laminar and dense (cortical or central) F-actin bundles or meshwork, they exhibited an increased ability to distort the cytoskeleton and breach the endothelial barrier at regions of relatively lower F-actin density. Thus, ILP probing by leukocytes seems to allow them to experience and sense local endothelial stiffness and thereby 'decide' where to transmigrate. Such path-of-least-resistance-seeking behavior might also be relevant in the subsequent egress across the basement membrane, during which leukocytes seem to seek out pre-existing weak spots in the matrix (Wang et al., 2006). Indeed, dendritic cells were recently shown to use podosomes to identify matrix 'soft' spots for progressive protrusion to facilitate more invasive antigen sampling (Baranov et al., 2014).

The relationship between tenertaxis and durotaxis

It is established that directed cell migration is crucially influenced by the mechanical properties of the substrate. In particular, increased stiffness of two-dimensional (2D) substrates promotes slower but more persistent directional migration (Discher et al., 2005; Pelham and Wang, 1998); Oakes et al., 2009). Furthermore, on 2D gradients of varied stiffness, many cell types exhibit lateral migration toward zones of greater stiffness, a process termed 'durotaxis' (from the Latin *duro* – hard, rigid, stiff) (Discher et al., 2005; Lo et al., 2000). Rigidity and stiffness mechanosensing during durotaxis requires RhoA- and myosin-II-mediated oscillatory cycles of contraction and relaxation applied to focal adhesions along the direction of migration. Here, "dynamic tugging serves as a means to repeatedly sense the local ECM rigidity landscape over time" to guide directed cell migration (Plotnikov et al., 2012; Plotnikov and Waterman, 2013; Raab et al., 2012).

The current findings focus on diapedesis. Although diapedesis is part of an overall process of highly directed cellular trafficking, it is fundamentally an invasive, barrier-breaching, pathfinding event as opposed to a true directed migration process. Thus, the role and mechanisms of sensing substrate and barrier mechanics might be fundamentally distinct in this setting. Indeed, we find here cells probing through a Cdc42/Rac1- and Arp2/3-mediated process (Carman, et al., 2007) of repeatedly extending and retracting ILPs in the direction normal to that of lateral migration in order to locally compress or push against (rather than pull on) the underlying cell substrate. Although podosomes have been suggested to be mechanosensitive (Albiges-Rizo et al.; Alexander et al., 2008; Collin et al., 2008), it remains to be determined whether tenertaxis is a bona fide mechanosensing process or a more simply stochastic one, in which breaching is limited by the local ILP-stalling force of the substrate (i.e. stiffness) combined with the overall efficiency of probing and lateral migration.

Thus, tenertaxis and durotaxis can be distinguished by context, the type or direction of force application and the cellular and molecular machinery implemented. These two processes should, therefore not be viewed as exclusive models, but rather as complementary context-specific modalities to survey the mechanical environment. Interestingly, two recent studies show for the first time that primary fibroblasts, which normally form robust focal adhesions and undergo directed cell migration, switch to ILP formation and invasive behavior on substrates with low stiffness (i.e. in a similar range to endothelial stiffness) (Gu et al., 2014; Yu et al., 2013).

MATERIALS AND METHODS

Reagents

Antibodies against the following rat proteins were used: ICAM-1 (1A29), VCAM-1 (5F10), [purified in-house as described previously (Adamson et al., 1999)], PECAM-1 (TDL-3A12), CD28 (JJ319) and CD3 (G4.18) from BD Pharmingen; and VEC (C-19) from Santa Cruz Biotechnology. Goat anti-mouse-IgG was from Sigma-Aldrich, Alexa-Fluor-647-conjugated donkey anti-goat-IgG, Alexa-Fluor-488–, Alexa-Fluor-594– and Alexa-Fluor-647–phalloidin and octadodecyl Rhodamine B chloride (R18) were from Invitrogen. Sources for antibodies against human αL (also known as ITGAL) (TS2/4) and ICAM-1 (CBR-IC1/11) have been described previously (Carman and Springer, 2004). Antibody against human VE-cadherin (clone 55-7H1) was from BD Biosciences; anti-PECAM-1 (clone 9G11) and polyclonal anti-VCAM-1 were obtained from R&D Systems. PP2 and histamine were from Sigma-Aldrich, adrenomedullin was from Bachem and 8-pCPT-2′-O-Me-cAMP (O-Me) was from Axxora. Recombinant rat and human TNF-α and IL2 were from Peprotech and R&D Systems, respectively. Collagenase and dispase were from Worthington Biochemical.

Endothelial cells

Primary rat cerebral endothelial cells were prepared and grown as described previously (Abbott et al., 1992; Romero et al., 2003). Primary cardiac endothelial cells were prepared from 5–7-week-old Lewis rats. Briefly, hearts were digested at 37℃ with collagenase (100 µg/ml), followed by a double selection with anti-PECAM-1 monoclonal antibody and sheep anti-rat-IgG Dynabeads™ (Invitrogen). The selection passage was repeated once the cells reached confluence. Human lung and cardiac microvascular endothelial cells were purchased from Lonza and maintained in EBM-2 with full supplements (Lonza). Cells were grown to confluence and treated with TNF-α (10 ng for 24 h) before application of the indicated stimuli.

T cells

Primary rat T cells were purified from spleen using $CD4^+$ MACS beads (Miltenyi) according to the manufacturer's instructions, cultured in CD3-coated plates in the presence of soluble CD28 and recombinant IL-2 for 72 h before expansion and further stimulation with IL-2 (25 U/ml). Human T-cells were separated by indirect magnetic labeling using the $CD4^+$ T cell isolation kit II (Miltenyi) according to the manufacturer's instructions and were cultured in the presence of human recombinant IL-2 (50 U/ml) in basic medium as described previously (Sage et al., 2012).

Plasmids and transfections

mYFP, pEGFP-actin and pEGFP-tubulin were purchased from Invitrogen. pEGFP-vimentin was a gift from Robert D. Goldman (Northwestern University, Evanston, IL). Membrane-targeted DsRed was generated by overlap-extension PCR to add an N-terminal palmitoylation sequence. Other DNA constructs were gifts from Keith Burridge (Rac1N17-GFP and RhoAN19-GFP; University of North Carolina, Chapel Hill, NC). MVEC transient transfection was performed by nucleofection according to the manufacturer's instructions (Amaxa). Experiments were conducted 48–72 h after transfection.

Journal of Cell Science (2014) 127, 3720–3734 doi:10.1242/jcs.148619

Immunofluorescence microscopy

TNF-α-treated confluent endothelial cells were treated with adrenomedullin or O-Me for 30 min and histamine or PP2 for 10 min prior to fixation, permeabilization and staining either with primary antibodies directly conjugated to Alexa Fluor or with non-conjugated primary antibodies followed by Alexa-Fluor-conjugated secondary antibodies. F-actin was detected with phalloidin–Alexa-Fluor-594 (Invitrogen). Rat T cells were detected with cholera-toxin–Alexa-Fluor-594 (Invitrogen).

Shear stress

TNF-α-treated confluent endothelial cells were exposed to 10 dyne/cm^2 of steady shear stress for 30 min or 48 h on an orbital rotator as described previously (Ley et al., 1989; Martinelli et al., 2009), applying the equation $\tau_{max}=\alpha\sqrt{\rho\eta(2\pi f)^3}$, where α is the radius of orbital rotation (2.5 cm), ρ is the density of the medium (1.0 g/ml), η is the viscosity of the medium (7.5×10^{-3} dynes•s/cm^2) and f is the frequency of rotation (rotations/second). Using this equation, a shear stress of 10 dynes/cm^2 is achieved at a rotating frequency of 125 rpm.

Measurement of barrier function by electrical resistance

Endothelial cells were grown to confluence on gold electrode plates, stimulated with TNF-α for 24 h before monitoring trans-endothelial electrical resistance (TEER) in real time by electric cell-substrate impedance sensing (ECIS) (Applied BioPhysics) (Tiruppathi et al., 1992). Resistance (Ω) values were analyzed by normalizing against baseline levels. Resistance per cm^2 (Ωcm^2) was calculated by multiplying the resistance values by the area of the electrodes used.

Measurement of barrier function by fluorescent tracer permeability

Barrier function was monitored with a quantitative imaging-based *in vitro* vascular permeability assay (Dubrovskyi et al., 2013) using a commercially available kit (Millipore), following the manufacturer's instructions. Briefly, six-well culture dishes were coated with a thin layer of biotinylated gelatin before seeding the endothelial cells. Once confluence was reached, TNF-α-treated endothelial cells were treated with drugs as indicated or exposed to 10 dyne/cm^2 of steady shear stress for 30 min or 48 h on an orbital rotator as described above. At the desired time-points, fluorescein–streptavidin (green; tetrameric molecular mass=211.2 kDa) was added for 5 min at room temperature, cells were washed, fixed, permeabilized and stained for VEC and actin. A total of 15 randomly selected fields were captured per condition by confocal microscopy (Zeiss). Permeability was calculated as the average mean background-subtracted fluorescence intensity of fluorescein–streptavidin per field, expressed as a percentage of the control condition, ±s.e.m.

Lymphocyte diapedesis

Confluent TNF-α-treated MVECs were prepared as described above and, where indicated, were further treated with adrenomedullin (10 µM, 30 min), O-Me (200 µM, 30 min), histamine (300 µM, 10 min), PP2 (2 µM, 10 min) or fluid shear conditioning (above). For migration experiments performed on substrates of different stiffness, endothelial cells were plated on elastically supported surface (ESS) dishes (Ibidi, µ-Dish$^{35\ mm,\ high}$ ESS) with stiffnesses of 1.5 kPa or 28 kPa. MVECs were briefly washed and species-matched T cells were added and allowed to migrate for either 10 min (all MVECs) or 30 min (rat brain MVECs only). Samples were fixed and stained, and quantification of diapedesis was performed by confocal microscopy as described previously (Carman et al., 2007). Briefly, three stages of migration were identified: 'apically adherent', 'transmigrating' (i.e. having breached the endothelial barrier) and 'under' the endothelium (i.e. having completed transmigration; see supplementary material Fig. S1A, schematic) based on relative distribution (assessed by confocal microscopy) of ICAM-1, VCAM-1 and LFA-1 and VE-cadherin or actin fluorescence in the x, y and z dimensions (Carman and Springer, 2004). More than ten fields per condition were imaged for a total of ≥100 cells per experimental replicate. 'Total diapedesis' (at a given time-point) was defined as follows: 'transmigrating'+'under'/the total number of cells (i.e. 'apically adherent'+'transmigrating'+'under')×100. The number of cells following each route of diapedesis was expressed as a percentage of 'transmigrating' cells.

Live-cell imaging

MVECs transfected with either actin–GFP, tubulin–GFP or vimentin–GFP and MemDsRed, were grown to confluence on Delta-T live-cell imaging dishes and stimulated with TNF-α, and live imaging was performed as described previously (Sage et al., 2012). In some cases, MVECs were incubated for 30 min with the membrane-permeable dye R18 and rinsed prior to live imaging. To determine the preferential area of T cell transmigration, lymphocytes were added in small numbers to the MVECs and individually followed until transmigration. Alternatively, MVECs were overloaded with T cells and, at the fixed time-point of 15 min, areas of transmigration were identified. The local endothelial actin, tubulin or vimentin intensity were calculated with Axiovision 4.6.3 software (Zeiss) at the preferential sites of migration per single migrating T cell and compared with the total intensity in the corresponding MVEC. Where indicated, MVECs were pre-treated with cytochalsin D (200 nM, 30 min) prior to performing migration experiments.

Atomic force microscopy

An atomic force microscope (AFM; MFP-3D Asylum Research on inverted optical microscope, Olympus IX51) was used to contact-mode image and then force-map living human lung MVEC junctions in complete medium at 37℃. Calibration of AFM cantilevers of nominal spring constant k=0.035 nN/nm and probe diameter of 600 nm (PT.Si02.SN.600; NovaScan) was conducted as described previously (Lee et al., 2010; Zeiger et al., 2012). Maps of force-depth responses over cell junctions (18×18 grid) were obtained for at least five junctions per condition, before and 15 min after drug treatment. Effective elastic moduli were calculated by applying a modified Hertzian elastic model to the loading segment of the force–depth response in Matlab (The Mathworks) as described previously (Lee et al., 2010; Zeiger et al., 2012). Elastic moduli are reported as the mean±s.e.m. of measurement.

Transmission electron microscopy

Transmission electron microscopy was performed as described previously (Carman et al.). In brief, TNF-α-activated endothelial cells grown on fibronectin-coated coverglass were incubated with T cells for the indicated times and then fixed with 2.5% glutaraldehyde and 2% paraformaldehyde in 1.0 M sodium cacodylate buffer pH 7.4 for 2 h, post-fixed in 1.5% sym-collidine-buffered OsO_4 for 1 h, stained en bloc with uranyl acetate, dehydrated in alcohol, and embedded in eponate. Thin eponate sections of 90 nm were cut with an ultramicrotome (Leica) and visualized with an electron microscope (CM-10; Philips) at an acceleration voltage of 60 kV. Images were taken on negative films. After development, the negative films were subjected to image scanning (using an Epson GT-X978 scanner and Epson File Manager software) and saved as TIFF files. Image brightness and contrast were adjusted in Adobe Photoshop software (CS4) and T cell and endothelial cell regions were highlighted with 15% opacity blue or green overlay, respectively, in Adobe Illustrator.

Statistical analysis

Data are presented as the mean±s.e.m. Variances of mean values were statistically analyzed by the Student's *t*-test. *$P<0.05$; **$0.001<P<0.01$; ***$P\leq0.001$.

Acknowledgements

We would like to acknowledge Francis William Luscinskas (Center for Vascular Biology Excellence, Brigham and Women's Hospital, Boston, MA) for providing vital reagents.

Competing interests

The authors declare no competing interests.

Author contributions

R.M. and C.V.C. designed and performed experiments; A.S.Z., M.W. and K.J.V.V. performed AFM experiments; T.E.S. and A.D. performed TEM experiments; R.M.,

A.S.Z., M.W., K.J.V.V. and C.V.C. analyzed data; R.M., C.V.C. and J.G. wrote the manuscript.

Funding

This work was supported by funding from the Wellcome Trust [grant number 062403 to J.G.]; the Rosetrees Trust (to J.G.); the American Heart Association (to C.V.C.); and the National Institutes of Health [grant number HL104006 to C.V.C.]. Deposited in PMC for immediate release.

Supplementary material

Supplementary material available online at
http://jcs.biologists.org/lookup/suppl/doi:10.1242/jcs.148619/-/DC1

References

Abbott, N. J., Hughes, C. C., Revest, P. A. and Greenwood, J. (1992). Development and characterisation of a rat brain capillary endothelial culture: towards an in vitro blood-brain barrier. *J. Cell Sci.* **103**, 23-37.

Adamson, P., Etienne, S., Couraud, P. O., Calder, V. and Greenwood, J. (1999). Lymphocyte migration through brain endothelial cell monolayers involves signaling through endothelial ICAM-1 via a rho-dependent pathway. *J. Immunol.* **162**, 2964-2973.

Albiges-Rizo, C., Destaing, O., Fourcade, B., Planus, E. and Block, M. R. (2009). Actin machinery and mechanosensitivity in invadopodia, podosomes and focal adhesions. *J. Cell Sci.* **122**, 3037-3049.

Alexander, N. R., Branch, K. M., Parekh, A., Clark, E. S., Iwueke, I. C., Guelcher, S. A. and Weaver, A. M. (2008). Extracellular matrix rigidity promotes invadopodia activity. *Curr. Biol.* **18**, 1295-1299.

Bamforth, S. D., Lightman, S. L. and Greenwood, J. (1997). Ultrastructural analysis of interleukin-1 beta-induced leukocyte recruitment to the rat retina. *Invest. Ophthalmol. Vis. Sci.* **38**, 25-35.

Baranov, M. V., Ter Beest, M., Reinieren-Beeren, I., Cambi, A., Figdor, C. G. and van den Bogaart, G. (2014). Podosomes of dendritic cells facilitate antigen sampling. *J. Cell Sci.* **127**, 1052-1064.

Bazzoni, G. and Dejana, E. (2004). Endothelial cell-to-cell junctions: molecular organization and role in vascular homeostasis. *Physiol. Rev.* **84**, 869-901.

Birukov, K. G., Birukova, A. A., Dudek, S. M., Verin, A. D., Crow, M. T., Zhan, X., DePaola, N. and Garcia, J. G. (2002). Shear stress-mediated cytoskeletal remodeling and cortactin translocation in pulmonary endothelial cells. *Am. J. Respir. Cell Mol. Biol.* **26**, 453-464.

Birukova, A. A., Arce, F. T., Moldobaeva, N., Dudek, S. M., Garcia, J. G., Lal, R. and Birukov, K. G. (2009). Endothelial permeability is controlled by spatially defined cytoskeletal mechanics: atomic force microscopy force mapping of pulmonary endothelial monolayer. *Nanomedicine* **5**, 30-41.

Bos, J. L. (2003). Epac: a new cAMP target and new avenues in cAMP research. *Natl. Rev. Mol. Cell Biol.* **4**, 733-738.

Caille, N., Thoumine, O., Tardy, Y. and Meister, J. J. (2002). Contribution of the nucleus to the mechanical properties of endothelial cells. *J. Biomech.* **35**, 177-187.

Carman, C. V. (2009). Mechanisms for transcellular diapedesis: probing and pathfinding by 'invadosome-like protrusions'. *J. Cell Sci.* **122**, 3025-3035.

Carman, C. V. and Springer, T. A. (2004). A transmigratory cup in leukocyte diapedesis both through individual vascular endothelial cells and between them. *J. Cell Biol.* **167**, 377-388.

Carman, C. V., Sage, P. T., Sciuto, T. E., de la Fuente, M. A., Geha, R. S., Ochs, H. D., Dvorak, H. F., Dvorak, A. M. and Springer, T. A. (2007). Transcellular diapedesis is initiated by invasive podosomes. *Immunity* **26**, 784-797.

Cinamon, G., Shinder, V., Shamri, R. and Alon, R. (2004). Chemoattractant signals and beta 2 integrin occupancy at apical endothelial contacts combine with shear stress signals to promote transendothelial neutrophil migration. *J. Immunol.* **173**, 7282-7291.

Collin, O., Na, S., Chowdhury, F., Hong, M., Shin, M. E., Wang, F. and Wang, N. (2008). Self-organized podosomes are dynamic mechanosensors. *Curr. Biol.* **18**, 1288-1294.

Cullere, X., Shaw, S. K., Andersson, L., Hirahashi, J., Luscinskas, F. W. and Mayadas, T. N. (2005). Regulation of vascular endothelial barrier function by Epac, a cAMP-activated exchange factor for Rap GTPase. *Blood* **105**, 1950-1955.

Dahl, K. N., Ribeiro, A. J. and Lammerding, J. (2008). Nuclear shape, mechanics, and mechanotransduction. *Circ. Res.* **102**, 1307-1318.

Dahl, K. N., Booth-Gauthier, E. A. and Ladoux, B. (2010). In the middle of it all: mutual mechanical regulation between the nucleus and the cytoskeleton. *J. Biomech.* **43**, 2-8.

Discher, D. E., Janmey, P. and Wang, Y. L. (2005). Tissue cells feel and respond to the stiffness of their substrate. *Science* **310**, 1139-1143.

Dubrovskyi, O., Birukova, A. A. and Birukov, K. G. (2013). Measurement of local permeability at subcellular level in cell models of agonist- and ventilator-induced lung injury. *Lab. Invest.* **93**, 254-263.

Dudek, S. M. and Garcia, J. G. (2001). Cytoskeletal regulation of pulmonary vascular permeability. *J. Appl. Physiol.* **91**, 1487-1500.

Fels, J., Jeggle, P., Liashkovich, I., Peters, W. and Oberleithner, H. (2014). Nanomechanics of vascular endothelium. *Cell Tissue Res.* **355**, 727-737.

Feng, D., Nagy, J. A., Pyne, K., Dvorak, H. F. and Dvorak, A. M. (1998). Neutrophils emigrate from venules by a transendothelial cell pathway in response to FMLP. *J. Exp. Med.* **187**, 903-915.

Gérard, A., van der Kammen, R. A., Janssen, H., Ellenbroek, S. I. and Collard, J. G. (2009). The Rac activator Tiam1 controls efficient T-cell trafficking and route of transendothelial migration. *Blood* **113**, 6138-6147.

Gu, Z., Liu, F., Tonkova, E. A., Lee, S. Y., Tschumperlin, D. J. and Brenner, M. B. (2014). Soft matrix is a natural stimulator for cellular invasiveness. *Mol. Biol. Cell.* **25**, 457-469.

Kis, B., Abraham, C. S., Deli, M. A., Kobayashi, H., Niwa, M., Yamashita, H., Busija, D. W. and Ueta, Y. (2003). Adrenomedullin, an autocrine mediator of blood-brain barrier function. *Hypertens. Res.* **26 Suppl.**, S61-S70.

Krishnan, R., Klumpers, D. D., Park, C. Y., Rajendran, K., Trepat, X., van Bezu, J., van Hinsbergh, V. W., Carman, C. V., Brain, J. D., Fredberg, J. J. et al. (2011). Substrate stiffening promotes endothelial monolayer disruption through enhanced physical forces. *Am. J. Physiol.* **300**, C146-C154.

Kvietys, P. R. and Sandig, M. (2001). Neutrophil diapedesis: paracellular or transcellular? *News Physiol. Sci.* **16**, 15-19.

Lee, S., Zeiger, A., Maloney, J. M., Kotecki, M., Van Vliet, K. J. and Herman, I. M. (2010). Pericyte actomyosin-mediated contraction at the cell-material interface can modulate the microvascular niche. *J. Phys. Condens. Matter* **22**, 194115.

Lelouard, H., Fallet, M., de Bovis, B., Meresse, S. and Gorvel, J. P. (2012). Peyer's patch dendritic cells sample antigens by extending dendrites through M cell-specific transcellular pores. *Gastroenterology* **142**, 592-601, e593.

Ley, K., Lundgren, E., Berger, E. and Arfors, K. E. (1989). Shear-dependent inhibition of granulocyte adhesion to cultured endothelium by dextran sulfate. *Blood* **73**, 1324-1330.

Ley, K., Laudanna, C., Cybulsky, M. I. and Nourshargh, S. (2007). Getting to the site of inflammation: the leukocyte adhesion cascade updated. *Nat. Rev. Immunol.* **7**, 678-689.

Lippmann, E. S., Al-Ahmad, A., Palecek, S. P. and Shusta, E. V. (2013). Modeling the blood-brain barrier using stem cell sources. *Fluids Barriers CNS* **10**, 2.

Lo, C. M., Wang, H. B., Dembo, M. and Wang, Y. L. (2000). Cell movement is guided by the rigidity of the substrate. *Biophys. J.* **79**, 144-152.

Lossinsky, A. S. and Shivers, R. R. (2004). Structural pathways for macromolecular and cellular transport across the blood-brain barrier during inflammatory conditions. *Histol. Histopathol.* **19**, 535-564.

Ludwig, T., Kirmse, R., Poole, K. and Schwarz, U. S. (2008). Probing cellular microenvironments and tissue remodeling by atomic force microscopy. *Pflugers Arch.* **456**, 29-49.

Lyck, R. and Engelhardt, B. (2012). Going against the tide – how encephalitogenic T cells breach the blood-brain barrier. *J. Vasc. Res.* **49**, 497-509.

Martinelli, R., Gegg, M., Longbottom, R., Adamson, P., Turowski, P. and Greenwood, J. (2009). ICAM-1-mediated endothelial nitric oxide synthase activation via calcium and AMP-activated protein kinase is required for transendothelial lymphocyte migration. *Mol. Biol. Cell* **20**, 995-1005.

Mehta, D. and Malik, A. B. (2006). Signaling mechanisms regulating endothelial permeability. *Physiol. Rev.* **86**, 279-367.

Muller, W. A. (2003). Leukocyte-endothelial-cell interactions in leukocyte transmigration and the inflammatory response. *Trends Immunol.* **24**, 326-333.

Müller-Redetzky, H. C., Kummer, W., Pfeil, U., Hellwig, K., Will, D., Paddenberg, R., Tabeling, C., Hippenstiel, S., Suttorp, N. and Witzenrath, M. (2012). Intermedin stabilized endothelial barrier function and attenuated ventilator-induced lung injury in mice. *PLoS ONE* **7**, e35832.

Pelham, R. J., Jr and Wang, Y. L. (1998). Cell locomotion and focal adhesions are regulated by the mechanical properties of the substrate. *Biol. Bull.* **194**, 348-349, discussion 349-350.

Pendyala, S., Usatyuk, P., Gorshkova, I. A., Garcia, J. G. and Natarajan, V. (2008). Regulation of NADPH oxidase in vascular endothelium: the role of phospholipases, protein kinases, and cytoskeletal proteins. *Antioxid. Redox Signal.* **11**, 841-860.

Pesen, D. and Hoh, J. H. (2005). Micromechanical architecture of the endothelial cell cortex. *Biophys. J.* **88**, 670-679.

Pfeiffer, F., Schäfer, J., Lyck, R., Makrides, V., Brunner, S., Schaeren-Wiemers, N., Deutsch, U. and Engelhardt, B. (2011). Claudin-1 induced sealing of blood-brain barrier tight junctions ameliorates chronic experimental autoimmune encephalomyelitis. *Acta Neuropathol.* **122**, 601-614.

Plotnikov, S. V. and Waterman, C. M. (2013). Guiding cell migration by tugging. *Curr. Opin. Cell Biol.* **25**, 619-626.

Plotnikov, S. V., Pasapera, A. M., Sabass, B. and Waterman, C. M. (2012). Force fluctuations within focal adhesions mediate ECM-rigidity sensing to guide directed cell migration. *Cell* **151**, 1513-1527.

Raab, M., Swift, J., Dingal, P. C., Shah, P., Shin, J. W. and Discher, D. E. (2012). Crawling from soft to stiff matrix polarizes the cytoskeleton and phosphoregulates myosin-II heavy chain. *J. Cell Biol.* **199**, 669-683.

Romero, I. A., Radewicz, K., Jubin, E., Michel, C. C., Greenwood, J., Couraud, P. O. and Adamson, P. (2003). Changes in cytoskeletal and tight junctional proteins correlate with decreased permeability induced by dexamethasone in cultured rat brain endothelial cells. *Neurosci. Lett.* **344**, 112-116.

Rotsch, C. and Radmacher, M. (2000). Drug-induced changes of cytoskeletal structure and mechanics in fibroblasts: an atomic force microscopy study. *Biophys. J.* **78**, 520-535.

Sage, P. T. and Carman, C. V. (2009). Settings and mechanisms for trans-cellular diapedesis. *Front. Biosci. (Landmark Ed.)* **14**, 5066-5083.

Sage, P. T., Varghese, L. M., Martinelli, R., Sciuto, T. E., Kamei, M., Dvorak, A. M., Springer, T. A., Sharpe, A. H. and Carman, C. V. (2012). Antigen recognition is facilitated by invadosome-like protrusions formed by memory/effector T cells. *J. Immunol.* **188**, 3686-3699.

Seltmann, K., Fritsch, A. W., Käs, J. A. and Magin, T. M. (2013). Keratins significantly contribute to cell stiffness and impact invasive behavior. *Proc. Natl. Acad. Sci. USA* **110**, 18507-18512.
Shulman, Z., Shinder, V., Klein, E., Grabovsky, V., Yeger, O., Geron, E., Montresor, A., Bolomini-Vittori, M., Feigelson, S. W., Kirchhausen, T. et al. (2009). Lymphocyte crawling and transendothelial migration require chemokine triggering of high-affinity LFA-1 integrin. *Immunity* **30**, 384-396.
Spindler, V., Schlegel, N. and Waschke, J. (2010). Role of GTPases in control of microvascular permeability. *Cardiovasc. Res.* **87**, 243-253.
Tee, S. Y., Bausch, A. R. and Janmey, P. A. (2009). The mechanical cell. *Curr. Biol.* **19**, R745-R748.
Tiruppathi, C., Malik, A. B., Del Vecchio, P. J., Keese, C. R. and Giaever, I. (1992). Electrical method for detection of endothelial cell shape change in real time: assessment of endothelial barrier function. *Proc. Natl. Acad. Sci. USA* **89**, 7919-7923.
Turowski, P., Martinelli, R., Crawford, R., Wateridge, D., Papageorgiou, A. P., Lampugnani, M. G., Gamp, A. C., Vestweber, D., Adamson, P., Dejana, E. et al. (2008). Phosphorylation of vascular endothelial cadherin controls lymphocyte emigration. *J. Cell Sci.* **121**, 29-37.
Vestweber, D. (2012). Relevance of endothelial junctions in leukocyte extravasation and vascular permeability. *Ann. N. Y. Acad. Sci.* **1257**, 184-192.
von Andrian, U. H. and Mackay, C. R. (2000). T-cell function and migration. Two sides of the same coin. *N. Engl. J. Med.* **343**, 1020-1034.
Wakatsuki, T., Schwab, B., Thompson, N. C. and Elson, E. L. (2001). Effects of cytochalasin D and latrunculin B on mechanical properties of cells. *J. Cell Sci.* **114**, 1025-1036.
Wang, K. and Sun, D. (2012). Influence of semiflexible structural features of actin cytoskeleton on cell stiffness based on actin microstructural modeling. *J. Biomech.* **45**, 1900-1908.
Wang, S., Voisin, M. B., Larbi, K. Y., Dangerfield, J., Scheiermann, C., Tran, M., Maxwell, P. H., Sorokin, L. and Nourshargh, S. (2006). Venular basement membranes contain specific matrix protein low expression regions that act as exit points for emigrating neutrophils. *J. Exp. Med.* **203**, 1519-1532.
Weiner, O. D., Marganski, W. A., Wu, L. F., Altschuler, S. J. and Kirschner, M. W. (2007). An actin-based wave generator organizes cell motility. *PLoS Biol.* **5**, e221.
Wojciak-Stothard, B. and Ridley, A. J. (2002). Rho GTPases and the regulation of endothelial permeability. *Vascul. Pharmacol.* **39**, 187-199.
Wolburg, H., Wolburg-Buchholz, K. and Engelhardt, B. (2005). Diapedesis of mononuclear cells across cerebral venules during experimental autoimmune encephalomyelitis leaves tight junctions intact. *Acta Neuropathol.* **109**, 181-190.
Yang, L., Froio, R. M., Sciuto, T. E., Dvorak, A. M., Alon, R. and Luscinskas, F. W. (2005). ICAM-1 regulates neutrophil adhesion and transcellular migration of TNF-alpha-activated vascular endothelium under flow. *Blood* **106**, 584-592.
Yu, C. H., Rafiq, N. B., Krishnasamy, A., Hartman, K. L., Jones, G. E., Bershadsky, A. D. and Sheetz, M. P. (2013). Integrin-matrix clusters Form podosome-like adhesions in the absence of traction forces. *Cell Rep.* **5**, 1456-1468.
Zeiger, A. S., Loe, F. C., Li, R., Raghunath, M. and Van Vliet, K. J. (2012). Macromolecular crowding directs extracellular matrix organization and mesenchymal stem cell behavior. *PLoS ONE* **7**, e37904.

Journal of Cell Science

Probing the Biomechanical Contribution of the Endothelium to Lymphocyte Migration: Diapedesis by the Path of Least Resistance.

Roberta Martinelli[1,2], Adam S. Zeiger[3], Matthew Whitfield[3], Tracey E. Scuito[4], Ann Dvorak[4], Krystyn J. Van Vliet[3,5], John Greenwood[2,‡] and Christopher V. Carman[1,‡]

Supplemental Figure Legends

Fig. S1. Assessing parameters of total lymphocyte migration, adhesion, endothelial cell geometry and adhesion molecule expression. (**a**) Schematic of stages of diapedesis. **(b)** 'Total Diapedesis'. Primary rat brain (rB), rat heart (rH), human lung (hL) and heart (hH) MVECs were grown to confluence and stimulated with TNF-α (24 h) before addition of rat or human T cells for 10 min (black bars; all ECs) or 30 min (white bars; rB only) to perform migration experiments. Samples were fixed, permeabilized, stained and quantified as described in *Material and Methods*. Data are the mean ± SEM of at least three separate experiments. (**c**) Cell area and junctional perimeter of primary rat brain (rB) and rat heart (rH) where calculated by manually tracing every cell in each field with the Axiovision software. Measurements were made for least three fields per cell type (cell n>15). (**d**) Primary rat brain and (**e**) rat heart MVECs were grown to confluence, stimulated with TNF-α (24 h) and treated with Adrenomedullin (AM, 10 μM) and 8-pCPT-2'O-Me-cAMP (O-Me, 200 μM) for 30 min and Histamine (His, 300 μM) and PP2 (10 μM) for 10 min prior to addition of T cells for adhesion or diapedesis experiments or (**f**) staining for surface expression of ICAM-1,

VCAM-1 and PECAM-1 and flow cytometric analysis. Data are the mean ± SEM of at least three separate experiments.

Fig. S2. Modulation of junctional integrity in hLMVECs and effects on diapedesis. hLMVECS were grown to confluence and stimulated with TNF-α (24 h) before addition of Adrenomedullin (AM, 10 μM), 8-pCPT-2'O-Me-cAMP (O-Me, 200 μM), Histamine (His, 300 μM) and PP2 (10 μM). (**a, b**) Human T cells were added for 10 min prior to adhesion or diapedesis experiments. (**c**) Changes in TEER are shown following treatments. Data are the mean ± SEM of at least four separate experiments. (**d**) Immunofluorescence imaging of hLMVECs following treatment with AM and O-Me for 30 min and His or PP2 for 10 min prior to fixation, permeabilization, staining for VEC (green) and F-Actin (red) (i) and quantitation of number of gaps per field (ii) and % of total gap area per field (iii) in PP2 and His treated cells. White arrowheads, cortical actin; yellow arrowheads, gaps. Scale Bars, 10 μm. Data are representative of at least five separate experiments. **(e)** hLMVEC were treated as above prior to addition of human T cells for 10 min followed by fixation, staining and quantitation for transcellular (i) and paracellular diapedesis (ii). Data are the mean ± SEM of at least four separate experiments.

Fig. S3. Assessing expression and distribution of adhesion molecules on hLMVEC following treatment with barrier-altering agents. (**a**) hLMVEC were grown to confluence and stimulated with TNF-α (24 h) before treatment with Adrenomedullin (AM, 10 μM) and 8-pCPT-2'O-Me-cAMP (O-Me, 200 μM) for 30 min and Histamine (His,

300 μM) and PP2 (10 μM) for 10 min prior to staining for surface expression of ICAM-1, VCAM-1 and PECAM-1 and flow cytometric analysis. (**b**) hLMVECs were grown to confluence and stimulated with TNF-α (24 h) prior to treatment as in (a). Cells were fixed and stained for ICAM-1, VCAM-1 and VEC or PECAM-1 and analysed by confocal microscopy. White lines indicate the area used for intensity analysis, which is shown in the corresponding line graphs below each image. Scale Bars, 10 μm. Data are representative of at least three different experiments.

Fig. S4. Characterization of fluid shear effects, fluorescence permeability assay, EC responses to substrate stiffness, ILP probing and Cytochalasin D treatment. **(a)** hLMVEC were grown to confluence, stimulated with TNF-α (24 h) and exposed to short or long shear (30 min or >36 h, respectively 10 dyne/cm^2). Shear was stopped and cells were fixed and stained for actin 10 min after shear cessation. Scale Bars, 10 μm (i). hLMVEC were shear pre-conditioned as in (i) and human T were added for 10 min under static condition then fixed, stained and imaged to quantify total diapedesis (ii). Data are the mean ± SEM of at least four separate experiments. **(b)** Endothelial permeability following treatment with Adrenomedullin (AM, 10 μM) or Histamine (His, 300 μM) was measured with a fluorescently based assay. Cells were fixed and imaged (i) and quantitation was performed as described in Materials and Methods (ii). **(c)** Human lung MVEC were grown to confluence either on glass (>10 GPa) or on elastic surfaces of 28 kPa and 1.5 kPa, stimulated with TNF-α (24 h) before fixation and staining for F-actin. **(d)** Live-cell imaging of T cell ILP probing on hLMVECs (i) or primary rat Brain MVEC (ii) that were grown to confluence, stimulated with TNF-α (24

h), stained with memR18 (to mark the plasma membrane). DIC (upper panels) and membrane fluorescence (lower panels) are shown. Note formation and disapperance of multiple fluorescent rings (i.e., 'podo-prints'; red arrows) reflective of T cell ILP formation. A transcellular pore (dashed yellow line) is shown in hLMVEC. Images are representative of at least four separate experiments. Scale Bars, 2 μm. **(e)** hLMVEC transfected with actin-GFP were grown to confluence, stimulated with TNF-α (24 h) and left untreated or treated with cytochalasin D (200nM, 30 min at 37ºC). Note the complete depletion of actin filaments throughout the cell body with maintenance of cortical actin at the inter-endothelial junctions. The images are representative of at least 7 separate experiments. Scale Bars, 10 μm.

Supplemental Movie Legends

Movie 1: Lymphocytes palpate the endothelium through invadosome-like protrusions (ILPs). Live-cell imaging of lymphocyte lateral migrating on MVEC transfected with memDsRed (magenta) and cytoplasmic-YFP (green). Parts I and II show a lymphocyte probing the endothelial cell junction or the cell body, respectively. Note the dynamic appearance and disappearance of circular rings of memDsRed fluorescence that correspond to cell surface invaginations ('podo-prints') reflective of invadosome-like protrusions (ILP) that are devoid of cytoplasmic-YFP. Images were acquired by time-lapse microscopy (Axiovert 200M; Carl Zeiss). Frames were taken every 30 s. See corresponding Fig.5c.

Movie 2: Frustrated ILPs probing on top of the nucleus. Live-cell imaging of a lymphocyte laterally migrating on MVEC transfected with mem-YFP (green). Note

appearance of multiple ‘non-productive/frustrated’ podo-prints/ILP probing on top of the nucleus, followed by appearance of ILP and a transcellular breach point immediately adjacent to the nucleus. Images were acquired by time-lapse microscopy (Axiovert 200M; Carl Zeiss). Frames were taken every 30 s. See corresponding Fig.7b.

Movie 3: Lateral T cell migration and ILP probing across endothelial junctions without diapedesis. Live-cell imaging of lymphocytes laterally migrating on MVEC transfected with memDsRed (magenta) and actin-GFP (green). Note three separate lymphocytes migrating laterally and avidly probing over a junction, without initiating a diapedesis event. Images were acquired by time-lapse microscopy (Axiovert 200M; Carl Zeiss). Frames were taken every 30 s.

Movie 4: Frustrated ILPs probing and failed diapedesis in zones of dense F-actin. Live-cell imaging of lymphocytes laterally migrating on MVEC transfected with memDsRed (magenta) and actin-GFP (green). Note the frustrated and prolonged probing of a lymphocyte in an actin-dense area (lower left) without breaching of the endothelium. Another lymphocyte succeeds in creating a transcellular pore, but it is unable to sufficiently deform the actin meshwork to allow for migration, resulting in a failed diapedesis attempt. Images were acquired by time-lapse microscopy (Axiovert 200M; Carl Zeiss). Frames were taken every 30 s. See corresponding Fig.8ai.

Movie 5: Avid ILP-mediated distortion of F-actin networks during lateral migration and ultimate diapedesis. Live-cell imaging of a lymphocyte laterally migrating on MVEC transfected with memDsRed (magenta) and actin-GFP (green). Note that in the zone of

modest F-actin density ILP probing causes appreciable bending and distortion of endothelial actin filaments, coupled to successful breaching of (and diapedesis across) the endothelium, when a zone of relatively reduced density of actin was reached. Images were acquired by time-lapse microscopy (Axiovert 200M; Carl Zeiss). Frames were taken every 30 s. See corresponding Fig.8b.

Movie 6: ILP-mediated endothelial cell breaching between two actin fiber to initiate diapedesis. Live-cell imaging of a lymphocyte laterally migrating on MVEC transfected with memDsRed (magenta) and actin-GFP (green). Note that the lymphocyte in a low F-actin density zone readily breaches and migrates across the endothelium by extending ILP between two actin filaments, which subsequently are 'bowed out' and distorted to accommodate completion of diapedesis. Images were acquired by time-lapse microscopy (Axiovert 200M; Carl Zeiss). Frames were taken every 30 s. See corresponding Fig.8aii.

Movie 7: Depletion of F-actin promotes avid transcellular diapedesis. Live-cell imaging of lymphocytes laterally migrating on MVEC that were transfected with memDsRed (magenta) and actin-GFP (green) and pre-treated with Cytochalasin D (200nM, 30 min) to deplete actin filaments. Note that actin filaments were profoundly lost within the endothelial cell body while a dense cortical actin ring was maintained at the junctions. In these conditions an extensive number of transcellular events can be seen, including several particular that were extremely close, but not migrating through the intact junction. See corresponding figure (Fig 8d) for post-fixation staining of VEC. Images

were acquired by time-lapse microscopy (Axiovert 200M; Carl Zeiss). Frames were taken every 20 s.

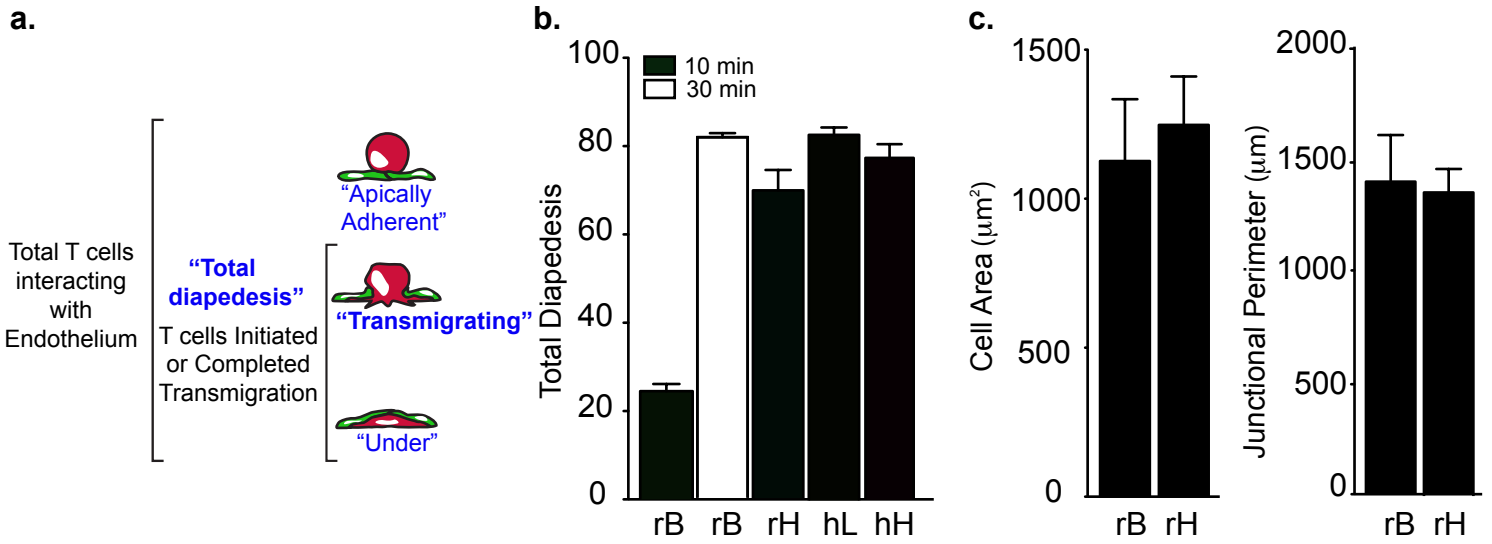
a.
Total T cells interacting with Endothelium
"Total diapedesis"
T cells Initiated or Completed Transmigration
"Apically Adherent"
"Transmigrating"
"Under"
b.
10 min
30 min
Total Diapedesis
rB rB rH hL hH
c.
Cell Area (μm²)
rB rH
Junctional Perimeter (μm)
rB rH

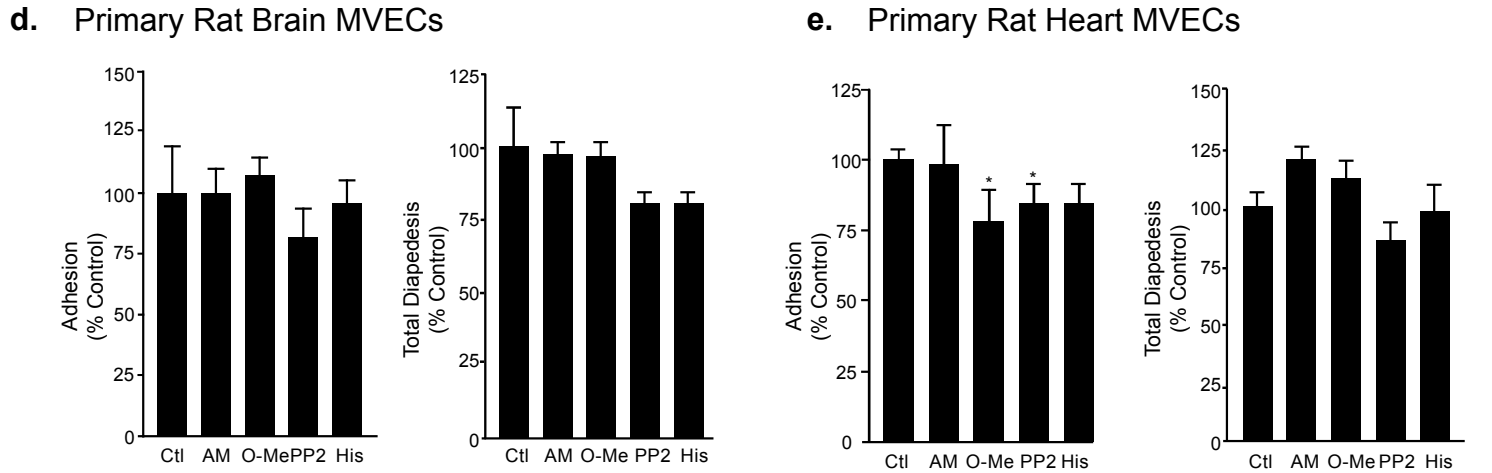
d. Primary Rat Brain MVECs
Adhesion (% Control)
Total Diapedesis (% Control)
Ctl AM O-Me PP2 His
e. Primary Rat Heart MVECs
Adhesion (% Control)
Total Diapedesis (% Control)
Ctl AM O-Me PP2 His

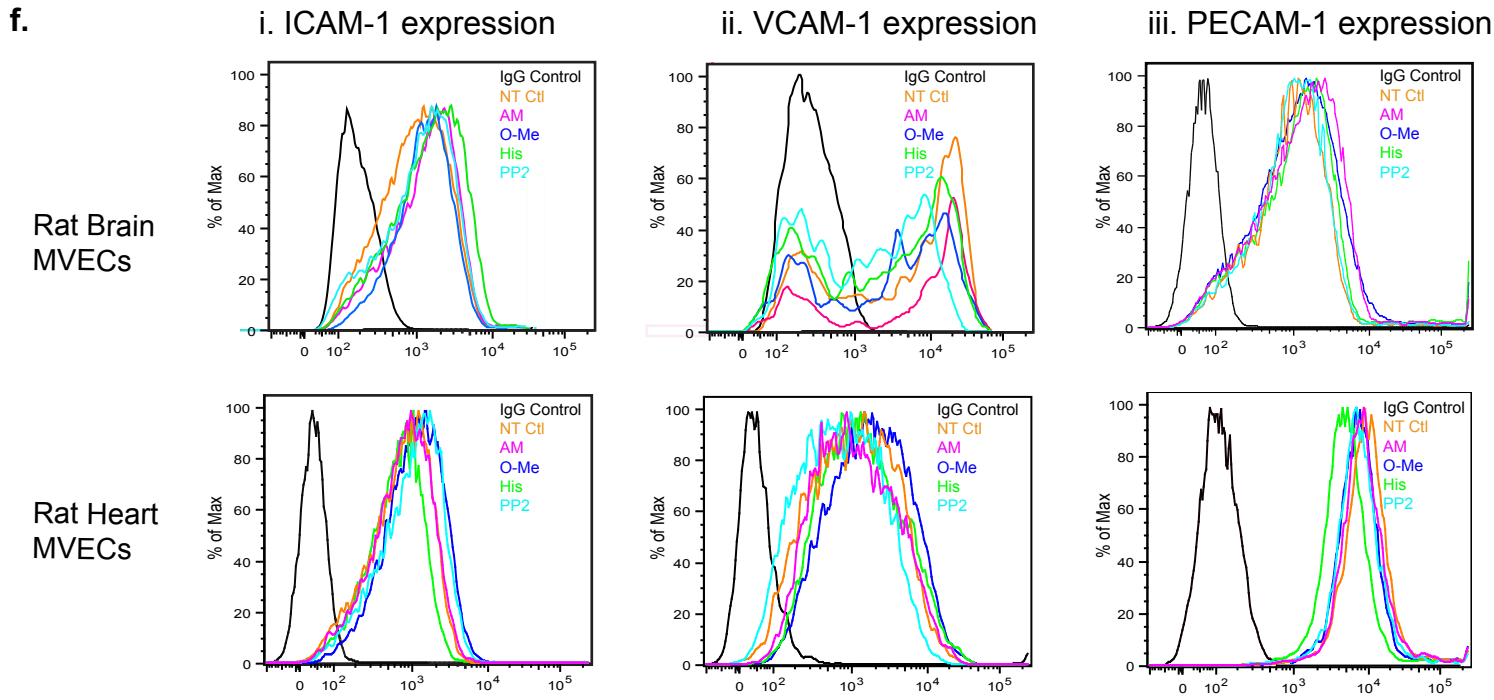
f.
i. ICAM-1 expression
ii. VCAM-1 expression
iii. PECAM-1 expression
Rat Brain MVECs
Rat Heart MVECs
% of Max
IgG Control
NT Ctl
AM
O-Me
His
PP2

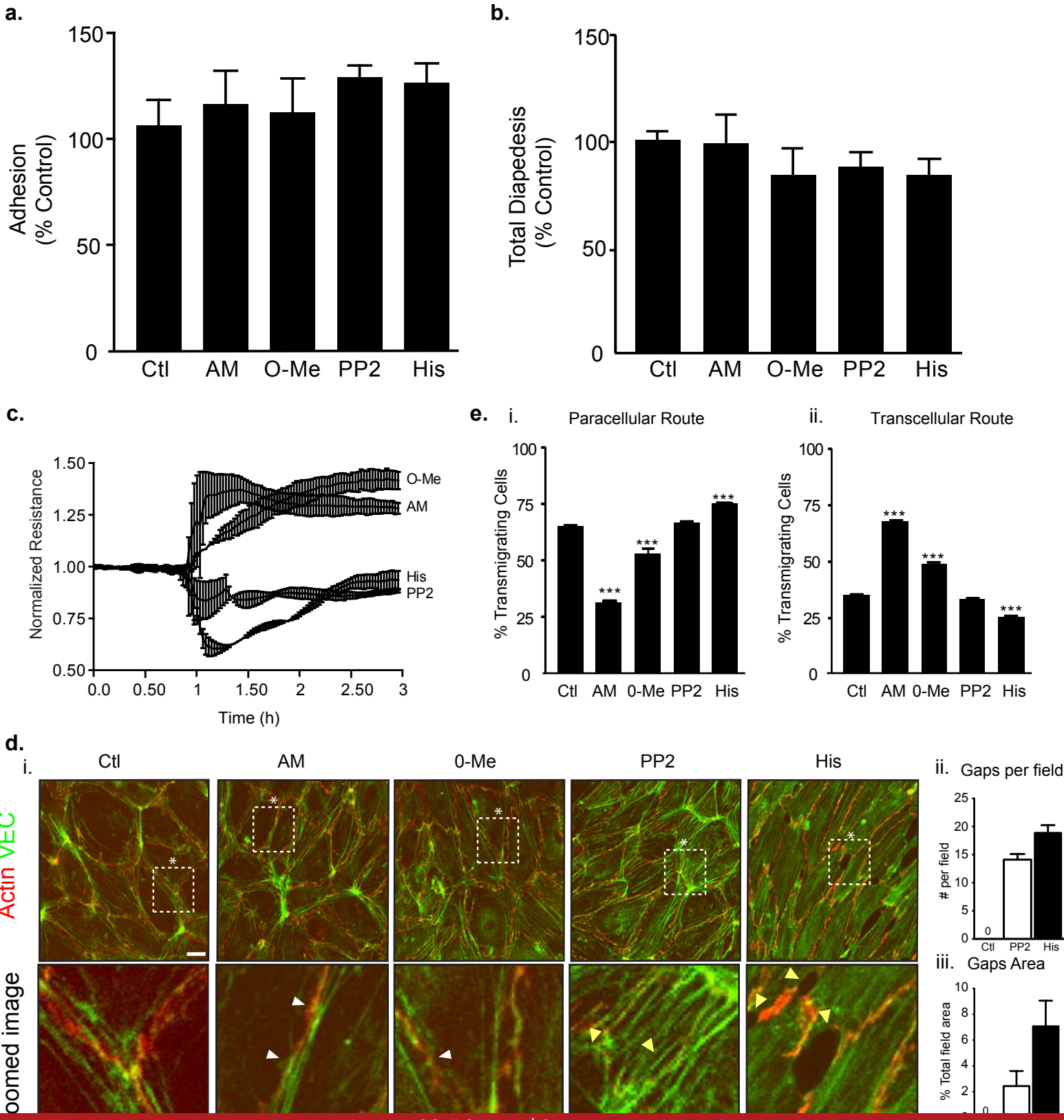
a.
Adhesion (% Control)
150
100
50
0
Ctl
AM
O-Me
PP2
His
b.
Total Diapedesis (% Control)
150
100
50
0
Ctl
AM
O-Me
PP2
His
c.
Normalized Resistance
1.50
1.25
1.00
0.75
0.50
0.0
0.50
1
1.50
2
2.50
3
Time (h)
O-Me
AM
His
PP2
e.
i.
Paracellular Route
% Transmigrating Cells
100
75
50
25
0
***
Ctl
AM
0-Me
PP2
His
ii.
Transcellular Route
% Transmigrating Cells
d.
i.
Ctl
AM
0-Me
PP2
His
Actin VEC
oomed image
ii.
Gaps per field
per field
25
20
15
10
5
0
Ctl
PP2
His
iii.
Gaps Area
% Total field area
10
8
6
4
2
0

a.

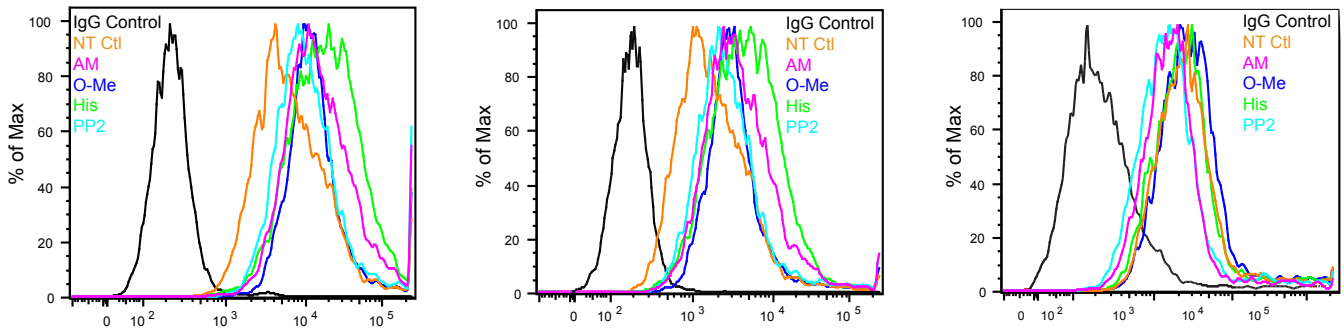
IgG Control
NT Ctl
AM
O-Me
His
PP2
% of Max

b.

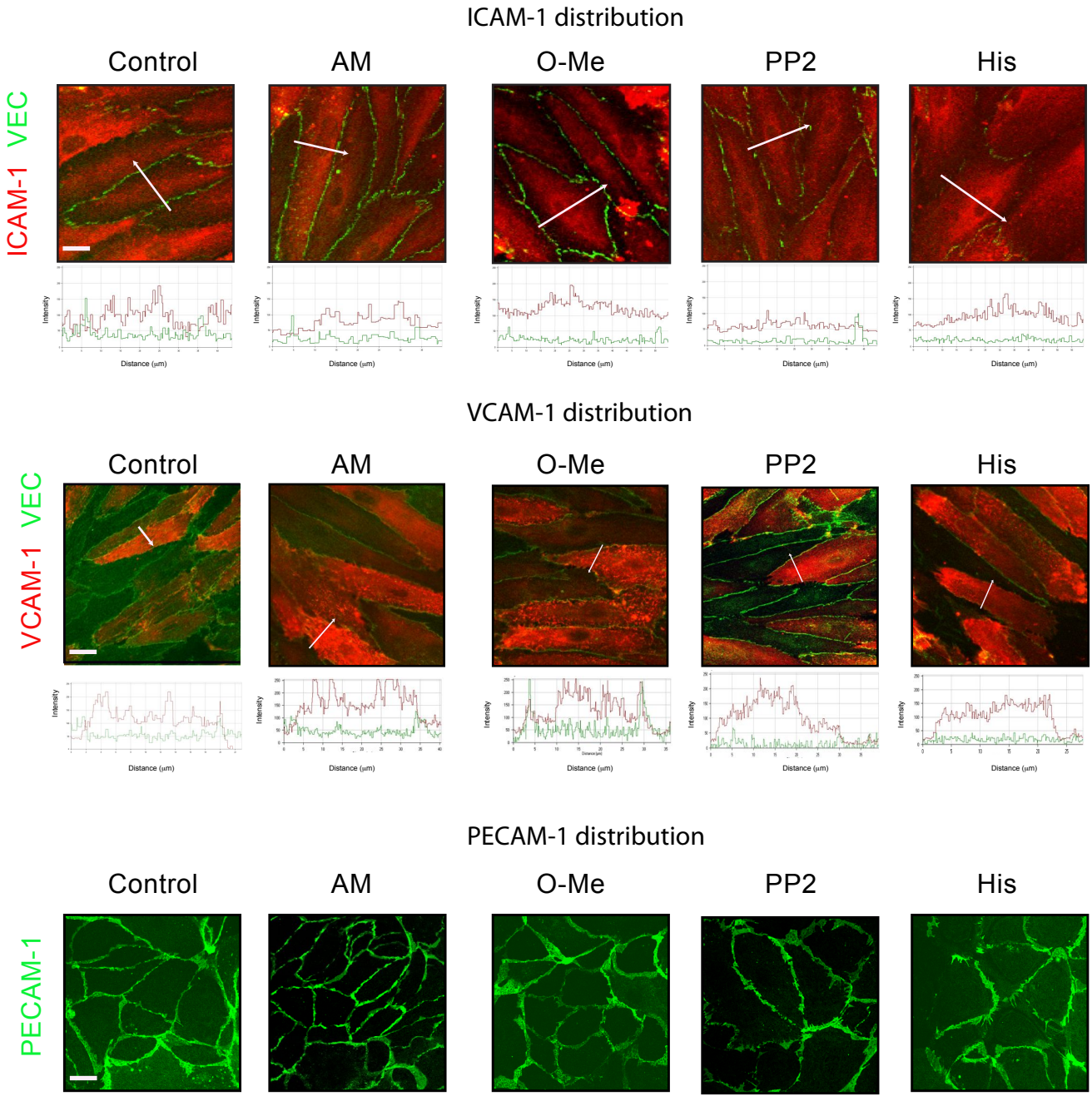
ICAM-1 distribution
Control
AM
O-Me
PP2
His
ICAM-1 VEC
VCAM-1 distribution
VCAM-1 VEC
PECAM-1 distribution
PECAM-1
Intensity
Distance (µm)

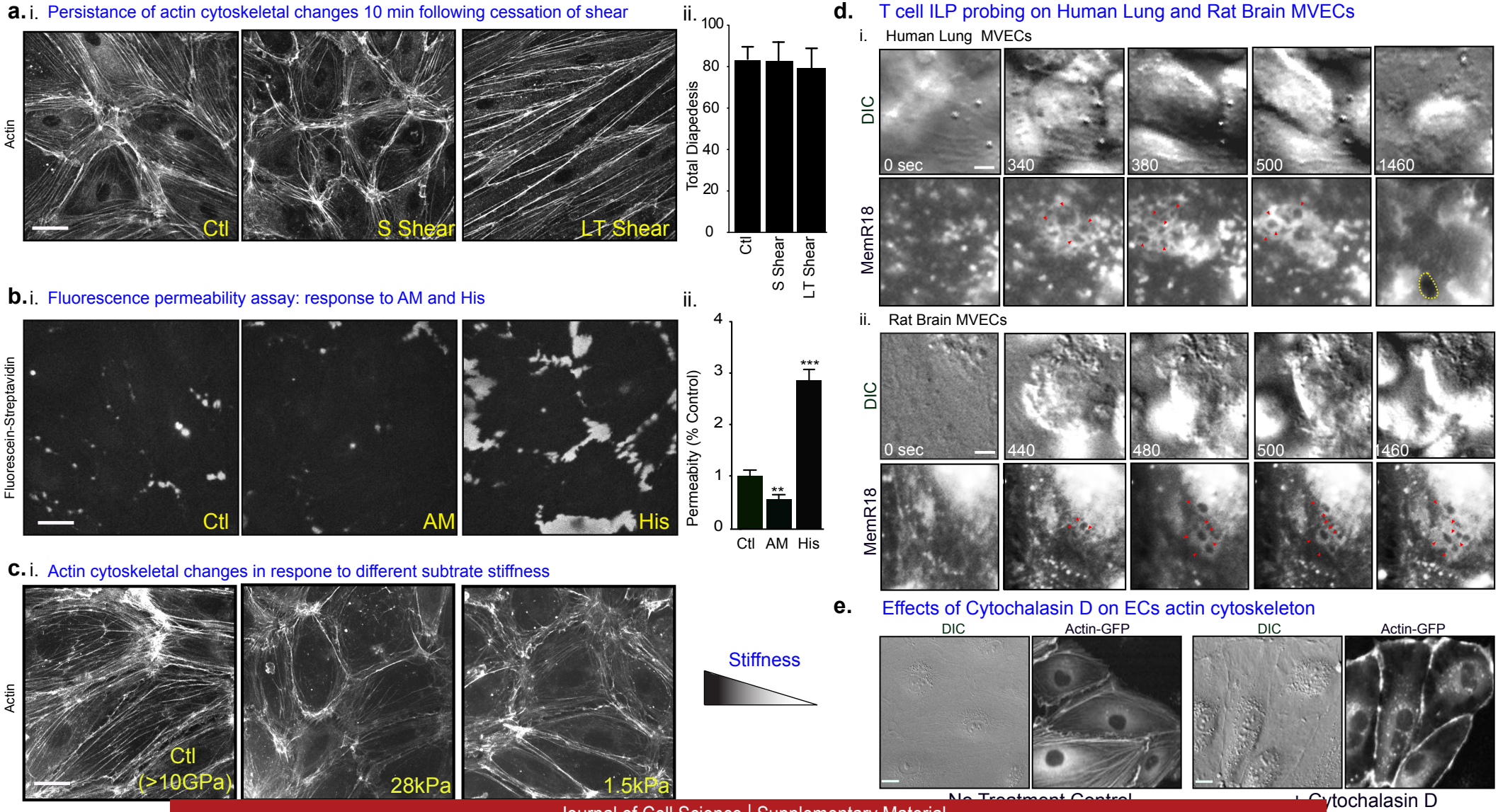
a. i. Persistance of actin cytoskeletal changes 10 min following cessation of shear
Actin
Ctl
S Shear
LT Shear
ii.
Total Diapedesis
100
80
60
40
20
0
Ctl
S Shear
LT Shear
b. i. Fluorescence permeability assay: response to AM and His
Fluorescein-Streptavidin
Ctl
AM
His
ii.
Permeabity (% Control)
4
3
2
1
0
**
***
Ctl
AM
His
c. i. Actin cytoskeletal changes in respone to different subtrate stiffness
Actin
Ctl
(>10GPa)
28kPa
1.5kPa
Stiffness
d. T cell ILP probing on Human Lung and Rat Brain MVECs
i. Human Lung MVECs
DIC
MemR18
0 sec
340
380
500
1460
ii. Rat Brain MVECs
DIC
MemR18
0 sec
440
480
500
1460
e. Effects of Cytochalasin D on ECs actin cytoskeleton
DIC
Actin-GFP
DIC
Actin-GFP
No Treatment Control
+ Cytochalasin D

Movie 1: Lymphocytes palpate the endothelium through invadosome-like protrusions (ILPs). Live-cell imaging of lymphocyte lateral migrating on MVEC transfected with memDsRed (magenta) and cytoplasmic-YFP (green). Parts I and II show a lymphocyte probing the endothelial cell junction or the cell body, respectively. Note the dynamic appearance and disappearance of circular rings of memDsRed fluorescence that correspond to cell surface invaginations ('podo-prints') reflective of invadosome-like protrusions (ILP) that are devoid of cytoplasmic-YFP. Images were acquired by time-lapse microscopy (Axiovert 200M; Carl Zeiss). Frames were taken every 30 s. See corresponding Fig.5c.

Movie 2: Frustrated ILPs probing on top of the nucleus. Live-cell imaging of a lymphocyte laterally migrating on MVEC transfected with mem-YFP (green). Note appearance of multiple 'non-productive/frustrated' podo-prints/ILP probing on top of the nucleus, followed by appearance of ILP and a transcellular breach point immediately adjacent to the nucleus. Images were acquired by time-lapse microscopy (Axiovert 200M; Carl Zeiss). Frames were taken every 30 s. See corresponding Fig.7b.

Movie 3: Lateral T cell migration and ILP probing across endothelial junctions without diapedesis. Live-cell imaging of lymphocytes laterally migrating on MVEC transfected with memDsRed (magenta) and actin-GFP (green). Note three separate lymphocytes migrating laterally and avidly probing over a junction, without initiating a diapedesis event. Images were acquired by time-lapse microscopy (Axiovert 200M; Carl Zeiss). Frames were taken every 30 s.

Movie 4: Frustrated ILPs probing and failed diapedesis in zones of dense F-actin. Live-cell imaging of lymphocytes laterally migrating on MVEC transfected with memDsRed (magenta) and actin-GFP (green). Note the frustrated and prolonged probing of a lymphocyte in an actin-dense area (lower left) without breaching of the endothelium. Another lymphocyte succeeds in creating a transcellular pore, but it is unable to sufficiently deform the actin meshwork to allow for migration, resulting in a failed diapedesis attempt. Images were acquired by time-lapse microscopy (Axiovert 200M; Carl Zeiss). Frames were taken every 30 s. See corresponding Fig.8ai.

Movie 5: Avid ILP-mediated distortion of F-actin networks during lateral migration and ultimate diapedesis. Live-cell imaging of a lymphocyte laterally migrating on MVEC transfected with memDsRed (magenta) and actin-GFP (green). Note that in the zone of modest F-actin density ILP probing causes appreciable bending and distortion of endothelial actin filaments, coupled to successful breaching of (and diapedesis across) the endothelium, when a zone of relatively reduced density of actin was reached. Images were acquired by time-lapse microscopy (Axiovert 200M; Carl Zeiss). Frames were taken every 30 s. See corresponding Fig.8b.

Movie 6: ILP-mediated endothelial cell breaching between two actin fiber to initiate diapedesis. Live-cell imaging of a lymphocyte laterally migrating on MVEC transfected with memDsRed (magenta) and actin-GFP (green). Note that the lymphocyte in a low F-actin density zone readily breaches and migrates across the endothelium by extending ILP between two actin filaments, which subsequently are 'bowed out' and distorted to accommodate completion of diapedesis. Images were acquired by time-lapse microscopy (Axiovert 200M; Carl Zeiss). Frames were taken every 30 s. See corresponding Fig.8aii.

Movie 7: Depletion of F-actin promotes avid transcellular diapedesis. Live-cell imaging of lymphocytes laterally migrating on MVEC that were transfected with memDsRed (magenta) and actin-GFP (green) and pre-treated with Cyto-chalasin D (200nM, 30 min) to deplete actin filaments. Note that actin filaments were profoundly lost within the endothelial cell body while a dense cortical actin ring was maintained at the junctions. In these conditions an extensive number of transcellular events can be seen, including several particular that were extremely close, but not migrating through the intact junction. See corresponding figure (Fig 8d) for post-fixation staining of VEC. Images were acquired by time-lapse microscopy (Axiovert 200M; Carl Zeiss). Frames were taken every 20 s.